Modelling and Simulation of a Fluidized Bed Membrane Reactor for Naphtha Reforming Process through Interfacing of Excel and Aspen-PLUS® Simulator

By

Adnan Ahmad Bhatti

School of Chemical and Materials Engineering (SCME)

National University of Sciences and Technology (NUST)

2019

Modelling and Simulation of a Fluidized Bed Membrane Reactor for Naphtha Reforming Process through Interfacing of Excel and Aspen-PLUS® Simulator

Adnan Ahmad Bhatti

2015-MS-CHE-03-00000117164

This work is submitted as an MS thesis in partial fulfillment of the requirement for the degree of

(MS in Chemical Engineering)

Supervisor Name: Dr. Iftikhar Ahmad

School of Chemical and Materials Engineering (SCME)

National University of Sciences and Technology (NUST)

2019

Dedicated to

My Parents and Siblings

Acknowledgments

First and foremost, praise be to Almighty Allah who showered me with His blessings and guided me in completing this task. This dissertation would not have been possible without the guidance and support of several individuals who in one way or another contributed and extended their valuable input in the preparation and completion of this study. I would like to extend my sincere gratitude towards my supervisor **Dr. Iftikhar Ahmad** for his timely guidance, patience and motivation throughout this research work. It was his unconditional support that helped me through so many roadblocks that I came across and it is difficult to say where I would be standing now without his help. I will always be grateful and appreciative of the assistance that he provided. I am also thankful to my guidance and examination committee members **Dr. Arshad Hussain**, and **Dr. Sarah Farrukh** for their valuable guidance. Last but not the least my appreciation also goes to the teachers of SCME and the class of 2015 that I was part of for the whole duration of my masters.

Adnan Ahmad Bhatti

Abstract

Naphtha reforming units are of great interest for hydrogen and gasoline production in petroleum refineries. Conventional reforming technology that employs packed-bed reactors (PBR) have inherent limitations that the fluidized bed reactor (FBR) overcomes. This study was conducted to assess the improvement in the yield of aromatics and hydrogen by the application of in situ membrane separation in the FBR. In this work, a sequential modular simulation (SMS) approach was used to simulate the hydrodynamics of a fluidized-bed membrane reactor (FBMR) for catalytic reforming of naphtha in the Aspen PLUS environment. Standard ideal reactor modules available inside the Aspen PLUS environment are combined to simulate the FBR and FBMR. The hydrodynamic parameters and membrane permeation phenomena were implemented using an interfacing of Excel with the Aspen PLUS model of the FBMR. Comparison of the results from the FBMR is done with a simulated FBR. FBMR outperformed the FBR in terms of increase in aromatics in reformate stream and effective separation of hydrogen during the reaction. The proposed method can be readily adopted by process engineers for design and optimization decisions.

Keywords: Naphtha catalytic reforming; Aspen PLUS; Excel interfacing; Two-phase theory of fluidization; Hydrogen production; Fluidized-bed membrane reactor; Increase in aromatic production; Pd–Ag membrane;

Nomenclature

A_c	reactor cross sectional area, m^2
CSTR	continuous stirred tank reactor
d_b	bubble diameter, m
E_i	energy of activation for the ith reaction, kJ/kmol
E_p	energy of activation of permeability, kJ/mol
FBP	final boiling point (^oC)
F^S_{H2}	shell side H_2 gas flow rate of in, kmol/h
F^t	total molar flow rate, kmol/h
H_2/Hc	hydrogen to hydrocarbon molar ratio
IBP	initial boiling point, ^oC
ICE	internal combustion engine
RON	research octane number
k_{ci}	coefficient for mass transfer of specie i, m/h
K_{ei}	equilibrium coefficient
k_{fi}	forward rate constant
L	length of reactor, m
MR	membrane reactor
PFR	Plug flow reactor
p_i	partial pressure of specie i, kPa
P_t	total pressure, kPa

p^{R}_{H2}	reaction side hydrogen partial pressure, Pa
p^{S}_{H2}	shell side hydrogen partial pressure, Pa
P	hydrogen permeability through Pd–Ag layer, mol/m^2 s $Pa^{1/2}$
P_0	pre-exponential factor of hydrogen permeability, mol/m^2 s $Pa^{1/2}$
R	ideal gas constant, kJ/kmol K
r_i	reaction rate for ith reaction, kmol/kg cat h)
T	temperature of gas phase, K
TBP	true boiling point, ^oC
t	time, h
u_b	velocity of rise of bubbles, m s^{-1}
C_{mp}	membrane permeation capacity (membrane surface area/thickness), km
E_p	activation energy for permeation, J mol^{-1}
k	pre-exponential factor, mol km^{-1} h^{-1} $Pa^{-0.5}$

Greek letters

α_H	hydrogen permeation rate constant, mol/m s $Pa^{0.5}$
d	thickness of palladium layer, mm
ρb	catalyst bed density, kg/m^3
ρg	density of gas phase, kg/m^3
v_{ij}	stoichiometric coefficient of specie i in reaction j
ΔH	heat of reaction, kJ/kmol

ε_b	void fraction of catalyst bed	
ε_{mf}	void fraction of catalytic bed at minimum fluidization	
ψ	catalyst particle shape factor	
δ	bubble phase volume as a fraction of total bed volume	(-)
η	membrane permeation effectiveness factor	(-)

Subscripts

a	aromatic
h	hydrogen
n	naphthene
p	paraffin

Table of Contents

List of Figures

List of Tables

Chapter-1

Introduction

1.1 Background

The catalytic reforming of naphtha is a process utilized for conversion of low-octane, straight-run naphtha into high-octane reformate which is then blended in gasoline to boost its octane rating. It is also a source of BTX (benzene, toluene, xylene isomers) which are important precursors for further chemical synthesis. A considerable amount of hydrogen gas is also produced in the process which is utilized in the refinery or other applications [1, 2]. Gasoline is still the fossil fuel of choice in terms of transportation even though it is now recognized as a source of global warming. In order to mitigate environmental concerns, various legislations are passed one of which is requirement of a high octane rating for motor gasoline [3].

Research octane number (RON) is the quality parameter of gasoline that shows how much compression it can withstand without knocking in a gasoline engine. The reforming process converts the low octane feed into a product with a high octane number. A high RON value around 100 denotes a fuel with good burning characteristics. Low octane hydrocarbons are unsuitable as an ICE fuel due to earlier detonation in a high compression engine. Newer high efficiency engines utilize high compression ratios and a fuel with a low RON value will detonate prematurely inside the engine cylinder thus causing the phenomena of knocking which is detrimental to engine life. High quality fuel thus should have a high RON value to make it suitable to be used in newer high compression engines.

Boosting of gasoline octane number is conveniently done by catalytic reforming of naphtha and it is carried out in three or four radial or axial flow fixed bed reactors. Mode of operation is semi-regenerative, cyclic or the newer continuous regenerative types. Another way of classification is done depending upon the severity of operation, and the regenerative procedure of catalyst. PBRs are used conventionally for naphtha reforming. It is a fixed bed type of reactor in which the catalyst is placed in a dumped arrangement. Catalyst

particle size cannot be reduced below a certain limit. Small diameter particles cannot be used due to excessive pressure drop [4]. Large particle size comes with disadvantages such as resistance to heat and mass transfer. Also, large particles have a low particle effectiveness factor. Thus, to overcome these limitations, catalyst particle size must be reduced.

Chemical reactants are shifted to products according to Le Chatelier's principle by selectively separating part of the reactant material from product gases [5,6]. One idea worth exploring is using a palladium membrane assisted fluidized catalyst bed reactor for naphtha reforming which is the focus of current study. A reactor configured in this way enables simultaneous, in situ removal of hydrogen from product gases, which increases the production of aromatics as the reactants pass through the reaction equipment. A simple reactor can be converted to a membrane reactor by replacing its outer wall with a perm-selective membrane material.

Various researchers have used membrane reactors for enhancement of product by shifting of thermodynamic equilibrium. Developing membrane reactor technology carries significance as a promising method for increasing hydrogen production by improving separation and recovery which will economize overall hydrogen production. In different studies palladium and its alloys such as palladium-copper, palladium-silver and pure palladium-based membranes were fitted inside conventional reactors [7, 8, 9, 10, 11]. For synthesis of methanol, Rahimpour proposed a membrane reactor with a pure Pd membrane [12]. Pasha developed Excel interfacing with Aspen PLUS to simulate an FBMR for steam reforming [33]. Tosti et al. carried out experiments to extract ultra-pure hydrogen by investigating the insertion of palladium-based membranes in different configurations inside conventional reactors [13]. One paper by Roy focuses on the simulation of membrane based fluidized bed reformers and its economic aspects [14]. Khosravanipour presented a concept of membrane assisted naphtha reformer and studied the effects of in situ hydrogen separation within a packed-bed reactor [15]. In another paper Rahimpour compared the results from a packed bed naphtha reformer with a fluidized bed membrane reformer [16].

Results presented show an enhancement of aromatics along the reactor. Hydrogen gas is generated as the naphtha reforming reaction proceeds in the reactor. Hydrogen separation from the product side could lead to the formation of dehydrogenation products which are associated with an increase in reformate RON. In another study, Rahimpour et al. simulated a thermally coupled reactor inside which two separate reactions, one endothermic and the other exothermic are occurring [17]. It was demonstrated that by this method the heat released by nitrobenzene to aniline conversion can be utilized by the heat requiring naphtha reforming reactions. All of the studies presented use MATLAB, FORTRAN or other software based modeling approaches that are not readily available to chemical engineers employed in the process design industry. Other than these theoretical studies not much have been explored and thus very few are available in the literature of fluidized-bed naphtha reformers with in situ hydrogen separation via membrane. Modeling of a membrane reactor is a challenging task because of simultaneous occurrence of diffusion coupled with mass transfer and chemical reaction inside the reactor [18].

Aspen PLUS is a widely employed process simulator for industrial process simulations in addition to various other simulation programs. In this study, an FBMR for naphtha reforming is developed on the Aspen PLUS platform with Excel interfacing. In an FBMR both physical and chemical phenomena coexist and need to be taken into consideration.

An adequate model for an FBMR should be able to represent the physical and chemical phenomena simultaneously. The physical phenomena are implemented by utilizing the hydrodynamics theory as an integrated sub model and chemical reactions are conveniently implemented by the built-in power law input panel of Aspen PLUS. Ideal reactor models are available as modules in Aspen PLUS and are combined together in a sequential manner in a certain way to mimic the behavior inside the fluidized bed membrane reactors [19]. Excel is used for calculation and transfer of the hydrodynamic parameters to the Aspen PLUS for calculation of volumes and voidage of the continuous stirred tank reactor (CSTR) and the plug flow reactor (PFR) blocks inside the flowsheet. Membrane permeation model is based on Sievert’s law.

1.2 Thesis Outline

This thesis comprises of work on development of an Aspen PLUS based model of a fluidized bed membrane reactor for the catalytic naphtha reforming

- The background for current work and the motivation for research is laid out in chapter 1.
- The reforming process is described in chapter 2. An industrial setup for a semi-regenerative reformer is taken as an example from literature where three packed bed reformers are used.
- Literature survey is presented in chapter 3.
- Chapter 4 details the model building and flow sheeting process in the Aspen PLUS environment with Excel interfacing.
- Results from the simulation are discussed and compared with FBR in chapter 5.

Chapter-2

Theoretical Background

Hydrocarbons comprise a large portion of crude oil a.k.a. petroleum, and account for nearly 97% by mass [1]. Further breakdown reveals paraffinic, naphthenic, and aromatic structures from light gases (methane, ethane, propane, butane) to waxy/asphaltenic matter collectively known as heaviers. The balance is made up of organic sulfur, oxygen, and nitrogen compounds. Water and salt are also found similar to the organometallic compounds of vanadium, sodium, and nickel. While the composition of several different compounds that make up a naphtha fraction wary widely among feed from different origins, carbon and hydrogen elemental composition does not vary by that much and is typically 85 %C and 15 % H_2. Carbon atom number of compounds usually range from C5 to C12 along with some nitrogen and sulfur. Naphtha is obtained as topmost fraction from atmospheric crude distillation unit and is called as straight run naphtha. Other portions of refinery also contribute to naphtha pool as a product of processing heavier crude fraction. Other compounds are also present in naphtha that is obtained from units other than atmospheric distillation units.

Naphtha is further divided among three fractions: one boiling between 30 ^oC and 90 ^oC is termed light naphtha and contains C5 to C6 hydrocarbons. The fraction that boils further till 20^oC from 90 ^oC is called heavy naphtha. An intermediate boiling stream that boils below 150 ^oC and contains C7 to C9 hydrocarbons is called medium naphtha. Table 2.1 shows sample naphtha composition from different geographic locations and gives an idea of relative amount of paraffin and naphthenes.

The feedstock of choice for a catalytic reforming unit is naphtha that has been desulfurized or hydrotreated. When benzene is desired then sometimes full range stocks are also used. Figure 2.1 shows a processing scheme followed in a refinery for production of gasoline with integrated catalytic reforming unit.

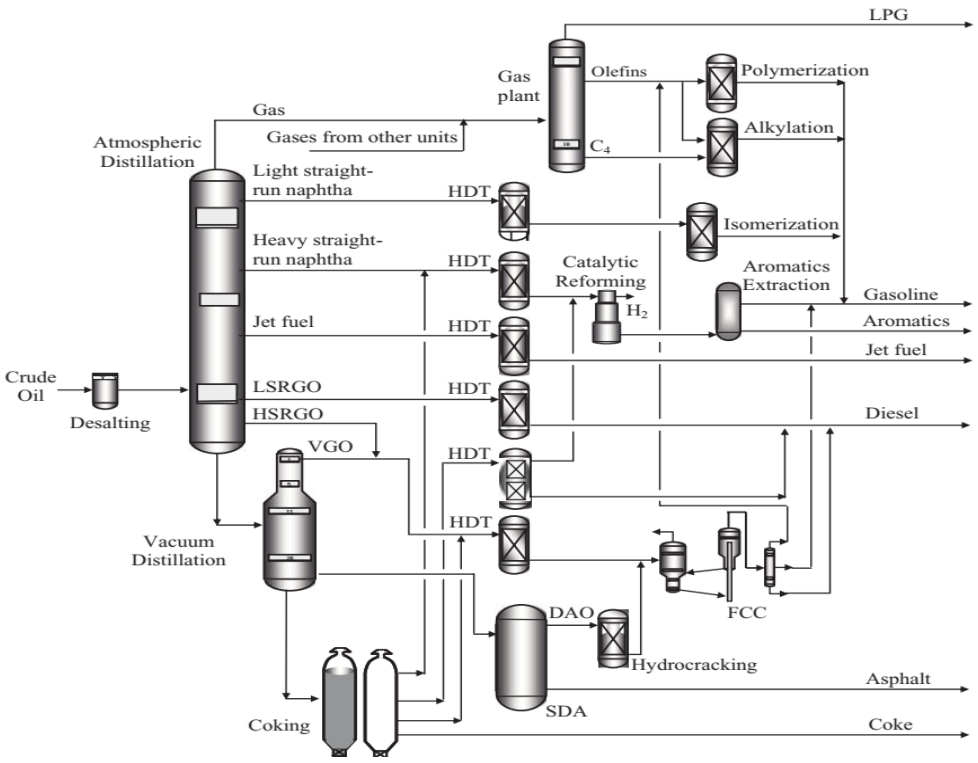

Figure 2.1: Typical Process Layout of a Petroleum Refining Unit

2.1 Composition of naphtha

The hydrocarbon component of naphtha is further divided into paraffin, naphthene and aromatic parts. Alkanes, commonly termed as paraffins, are saturated hydrocarbons of aliphatic nature and their carbon and hydrogen composition can be represented by C_nH_{2n+2}. Presence of branching differentiates iso and normal paraffins. Normal paraffins always have higher boiling points as compared to their isomeric counterparts in the same carbon atom range. Boiling point and density increases with carbon number. Unsaturated, aliphatic hydrocarbons which may be straight or branched and contain a double bond are called olefins. Naphthenes and aromatics are both cyclic compounds of carbon. The difference is that the naphthenes are saturated and the aromatics contain conjugate double bonds. BTX (benzene toluene, and xylene isomers) are important feedstock for the petro industry and high research octane numbers.

Table 2.1: Naphtha composition from around the world [1]

Oil field	Paraffins (wt %)	Naphthenes (wt %)	Aromatics (wt %)	Sulfur (wt ppm)	Nitrogen (wt ppm)
Troll (Norway)	13.9	75.2	10.8	20	<1
Norne (Norway)	27.7	34.8	37.5	10	<1
Tehran (Iran)	72	17.1	10.9	<10	<1
Leufeng (China)	69.5	27.5	2.9	<10	1

Table 2.2: Compositions and Properties of Refinery Naphtha Streams Originating from the Crude Oil of a typical oil well [1]

Stream	Olefins (wt %)	Paraffins (wt %)	Naphtha (wt %)	Aromatics (wt %)	Density (kg/m^3)	IBP–FBP (^OC)	Crude (wt %)
Light SR	—	55	40	5	664	C_5–90	3.2
Medium SR	—	31	50	19	771	90–150	8.6
Heavy SR	—	30	44	26	797	150–180	4.7
FCC	23	34	11	32	752	C_5–220	20
Light VB	10	64	25	1	667	C_5–90	—

Heavy VB	30	46	16	8	750	90–150	—

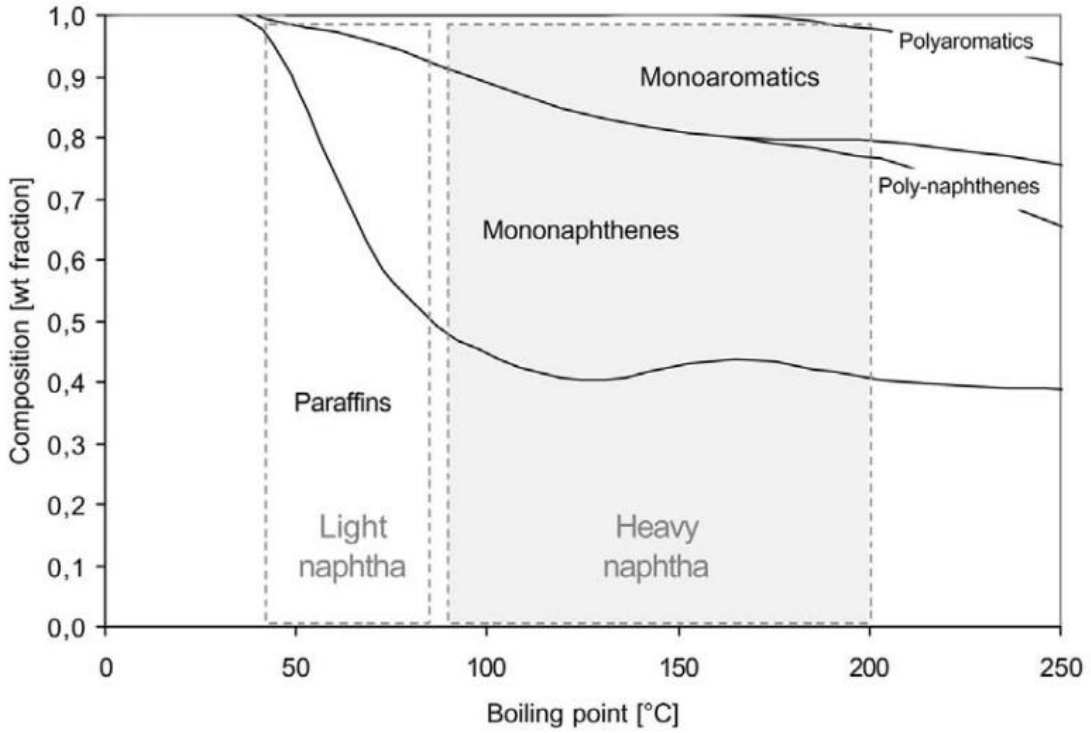

Figure 2.2: Composition of Hydrocarbons vs Boiling Point Obtained from Distillation of a North Sea Crude

Sulfur may be present in a quantity of up to 5% in crude oil and is an important hetero-atom. Heavy crude oil fractions typically contains the highest amount of sulfur. Straight run naphtha has only minor ppm levels of sulfur. Presence of sulfur is of concern whether the feedstock is used for reforming or as a fuel. If sulfur containing feed is sent to reformer, then it can poison the Pt catalyst. If it is used as fuel, then its combustion can yield oxides of this element that are environmental pollutants. Sulfur removal can be accomplished by its conversion to hydrogen sulfide in a process known as hydrotreating. Some representative sulfur compounds identified from crude oil analysis are shown found in Figure 2.3.

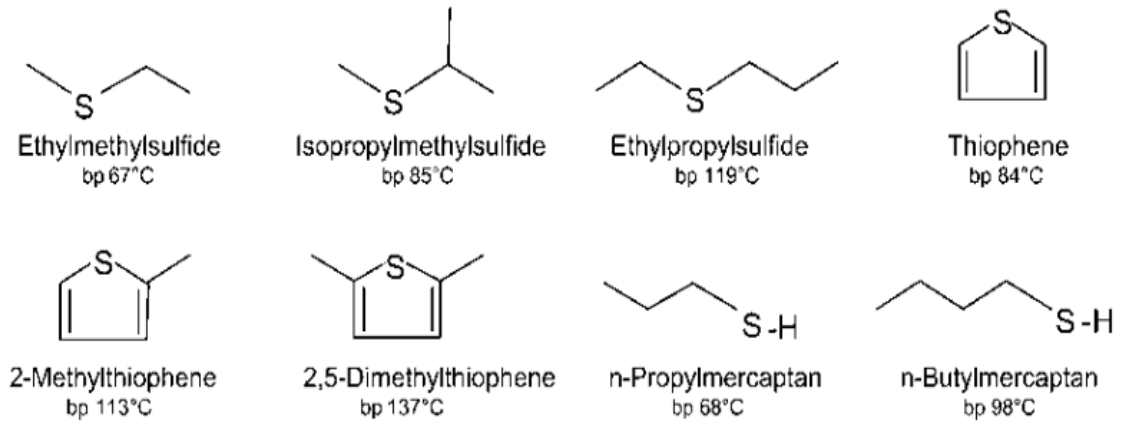

Figure 2.3: Structure of few sulfur compound found in naphtha

Organic compounds of nitrogen are also present mixed among higher boiling fractions of crude oil although their quantity is even less than sulfur compounds. Nitrogen is a poison for acidic part of reforming catalyst Some representative compounds are depicted in Figure 2.4.

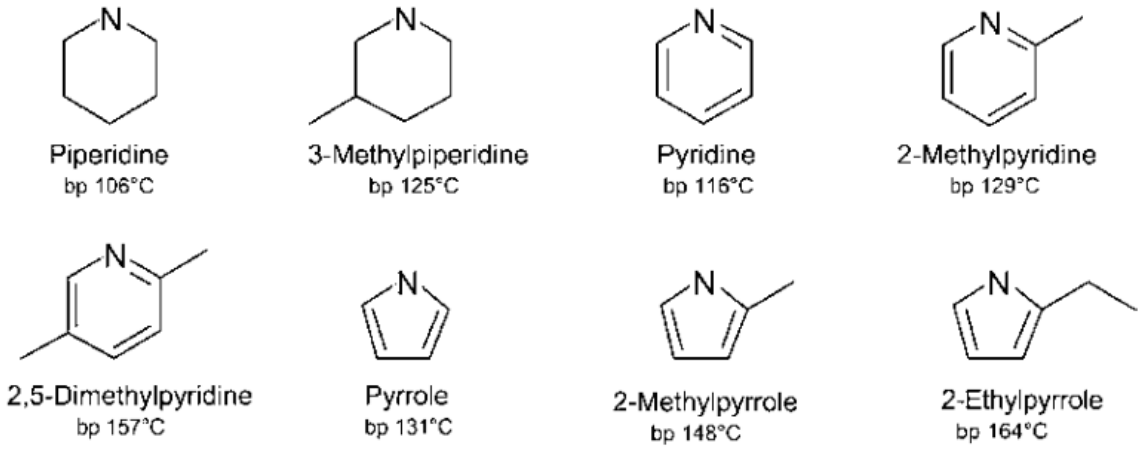

Figure 2.4: Structure of nitrogen compounds found in straight-run naphtha

Normally naphtha is nearly free of organic compounds of oxygen and they are usually present in heavier fractions of crude. Their presence is mainly a concern for corrosion.

Some water may also be present in the crude oil. It can be present in water-in-oil emulsion and also as free water. Problems can arise if naphtha contains dissolved moisture as it has high latent heat of vaporization and a nuisance during distillation. Heavy organometallic compounds are not a part of boiling point fraction which is in the naphtha range. Mostly are results of corrosion of containment vessels. Silicon compounds can damage the catalyst.

2.2 Process Description

During the reforming process, the low-octane hydrocarbons present in the feed are modified or *reformed* to yield high value reformate. During the reconstruction, the boiling point range of naphtha does not change significantly [2]. Typically, 3-4 serially connected fixed-bed reactors are employed for reforming with inter-stage heating. The feed gas is pre-heated with heat exchange from the effluent of the last reactor. Heat exchangers are usually of shell and tube type. As the reforming reactions are endothermic, effluent from each reactor requires reheating to compensate for temperature drop and related rate of reaction decline.

Figure 2.5 shows the process flow diagram of naphtha reforming process. The feed and recycle hydrogen is mixed in a calculated mole ratio to maintain the H_2/Hc ratio around 4 and preheated by products from the final reactor. The preheated feed is brought to the reaction temperature of 777 K in the feed heater and fed to the first reactor. Reactors are loaded with Pt-Re catalysts on an alumina support. The catalyst is bi-functional, the alumina provides acid function and Pt-Re provides the metal function for dehydrogenation of naphthenes.

The partially reacted effluent from reactor 1 is brought up to reaction temperature in heater 2 and becomes feed to reactor 2. With the passage through reactors, rates of reaction drop resulting in increased reactor volume. There is also a notable decrease in endothermicity of reactions and consequently the heat requirement also decreases. The product from the third reactor first exchanges heat with the incoming feed where it is cooled and the feed is pre-heated. After further cooling in the product cooler the product is sent to the flash

separator vessel where the liquid and gaseous components are separated. Cooling of product stream is required due to its high temperature. A drop in temperature affects the separation of lighter gases from reformate liquid. Flashed-gas contains most part hydrogen along with products of cracking mainly small quantity of light gases namely methane, ethane, propane, and butanes.

The hydrogen from flash separator is split into two parts. One part is compressed and added to naphtha feed to maintain inlet H2/Hc ratio. The other part is sent to LPG extraction unit. Bottom product from the flash separator needs stabilization before it is sent to reformate storage.

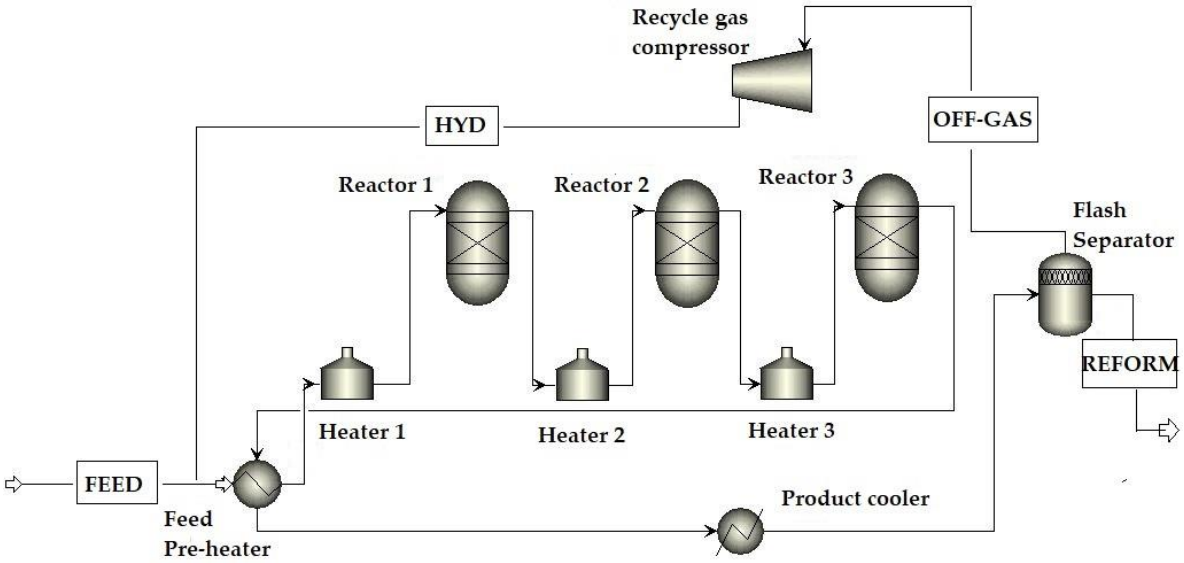

Figure 2.5: Catalytic naphtha reforming process as a PFD

The focus of the current study is the first reactor where the dominant reaction is dehydrogenation of alkylcyclohexanes to their corresponding aromatics. The dehydrogenation reaction is the main reaction responsible for the rise of RON value [20]. A temperature drop of almost 50 ^{o}C is observed in the first reactor which essentially quenches other reactions and requires reheating of reactants.

2.3 Reaction kinetics of naphtha reforming process

A bi-functional catalyst is employed for the reforming process. The two functions are actually metallic and acidic in nature and are needed for different reactions. Hydrogenation and dehydrogenation reactions are catalyzed by the metal function and the acid function promotes the cyclization and isomerization reactions [21–23]. The dehydrogenation reaction which is the dominant reaction has been focus of a number of studies and is reported in the literature. The first study reported was from Smith in 1959 which included the dehydrogenation reactions in his 4 lumped model [24]. Other variations of Smith's model have been proposed later with the passage of time.

Marin et al. (1983) have performed detailed studies regarding reforming kinetics and have included pertinent reactions [25-30]. All their studies are based on lumped kinetic schemes. An appropriate model was proposed by Padmavathi and Chaudhuri (1997) using a lumped kinetic scheme [31]. Their model has some weaknesses; they have excluded some important reactions and have used a simplified lumping scheme.

Industrially, the product of main interest are aromatic components and the sub-division of 8-carbon aromatics needs to be taken into account. Other important reactions namely paraffin to aromatic dehydrocyclyzation, transalkylation and isomerization of aromatics have not been taken into account. New to this improved model, is the further sub-division of 8-carbon aromatics into four components (ethyl benzene, and ortho, meta and para isomers of xylene) along with their respective variation are taken into account [32]. The dehydrogenation reaction scheme is presented in Table 2.3. along with reported rates of reaction.

In addition to the modeling of the reaction kinetics the reactor design has been the focus of the research. A fluidized bed reactor (FBR) was proposed by Rahimpour to replace the conventional reactor. The idea behind the use of FBR is to use catalyst particles in 100 micron range to eliminate inner mass transfer resistance combined with negligible pressure drop due to fluidization. In recent studies the transformation of FBR into a membrane based fluidized bed reactor has been proposed [16, 17].

Table 2.3: Dehydrogenation reactions with rate constant and heat of reaction data

$\mathbf{ACH} \leftrightarrow \boldsymbol{A_n} + \mathbf{3H_2}$	$r_{1n=}k_{1n}\left(P_{ACHn} - \frac{P_{An}P_{H2}^3}{K_{1n}}\right)$	$k_{1n} = exp\left(a - \frac{E}{RT}\right)$ $(kmol.kg_{cat}^{-1}.h^{-1}.kPa^{-1})$		$K_{1n} = exp\left(A - \frac{B}{T}\right)$ $(kPa)^3$	
	$\triangle H\left(\frac{kJ}{molH_2}\right)$	a	$\frac{E}{R}$	A	B
C_6	68.73	18.75	19500	59.90	24800
C_7	208.47	20.70	19500	60.23	25080
C_8					
for A_n = MX*	64.50	17.89	19500	60.37	23270
for A_n = MX*	65.10	19.15	19500	60.32	23490
for A_n = MX*	64.74	18.66	19500	60.13	23360
for A_n = MX*	68.70	18.71	19500	60.40	24780
C9+	66.05	20.38	19500	61.05	21330

* improvements made to the Padmavathi et al. model.

2.4 Fixed-bed process

A fixed-bed reactor is a common type of reactor utilized for heterogeneous catalytic reactions. Typically, it is a large cylindrical vessel or a column filled with random/dumped packing material. The packing material has surface treatments done so it acts both as a catalyst and enhances fluid-solid contact. Reactants are present either present in a single phase in a homogeneous system or in different phases in a heterogeneous system. Flow of reactants is from the top of the bed to prevent fluidization of the catalyst in a heterogeneous solid catalyzed system. The fluid has to flow through the packing material and this causes a pressure drop in an axial flow reactor. Radial flow reactors have a comparatively lower pressure drop as compared to axial flow reactors but the problem of uneven reactant distribution is an issue. Using a large packing size to prevent a high pressure drop introduces mass transfer resistances. To reduce the effects of packing and to improve the

flow the packing is distributed in an open cage-like structure which increases the size of the vessel. For high pressure vessels this increase in size correlates to an increase in cost.

2.5 Fluidized-bed process

The fluidization process is a method for intimate contacting of a finely ground solid such as catalyst particles with a fluid such as a gas. Figure 2.6 (a) shows what happens when a fluid such as a gas is passed upward from the bottom at a low flowrate through a fixed bed of fine particles. This results in the percolation of gas through the interstities between stationary particles. As the flowrate is increased, particles tend to vibrate in a restricted manner and start moving apart. The bed is now just starting to expand.

As the gas velocity is increased at a certain point all the particles become stationary due to the upward movement of gas. The weight of the particles is now exactly balanced by the frictional force between the particles and the flowing gas, adjacent particles no longer have a vertical component of compressive force, and the pressure drop through any section of the bed almost becomes same as the weight of gas and particles in that section. The bed is now in a state referred to as just fluidized and is known as an incipiently fluidized bed or a bed at minimum fluidization.

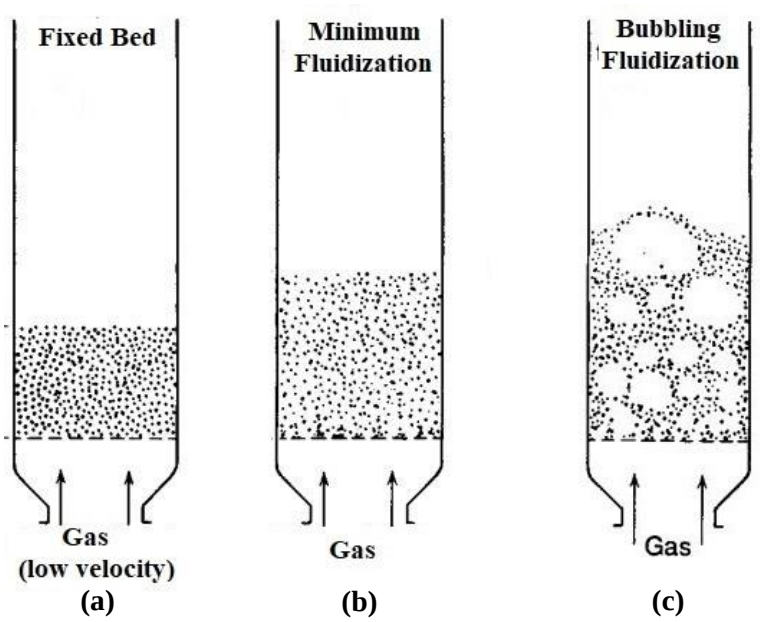

Figure 2.6: Different gas-solid contacting patterns in a fluidized bed

To fluidize a fixed-bed the catalyst particles are crushed to a small size of about 100 microns. During the reforming process heat and mass transfer occurs within the reactor a hydrogen partial pressure gradient is set up which results in a net transfer of hydrogen to the shell side. This transfer of excess hydrogen results in displacing the reaction to the formation of more product.

The fluidization of catalyst particles is carried out by feeding the catalyst filled reactor with gas from bottom through a porous plate distributor. Hydrogen is used as the sweep gas in the shell compartment where its flow is co-current with the reacting gas. The pressure drop in a fluidized bed is very low even though a very small catalyst size is used that would not be feasible in a fixed bed. The phenomena inside an FBMR is shown in Figure 2.7.

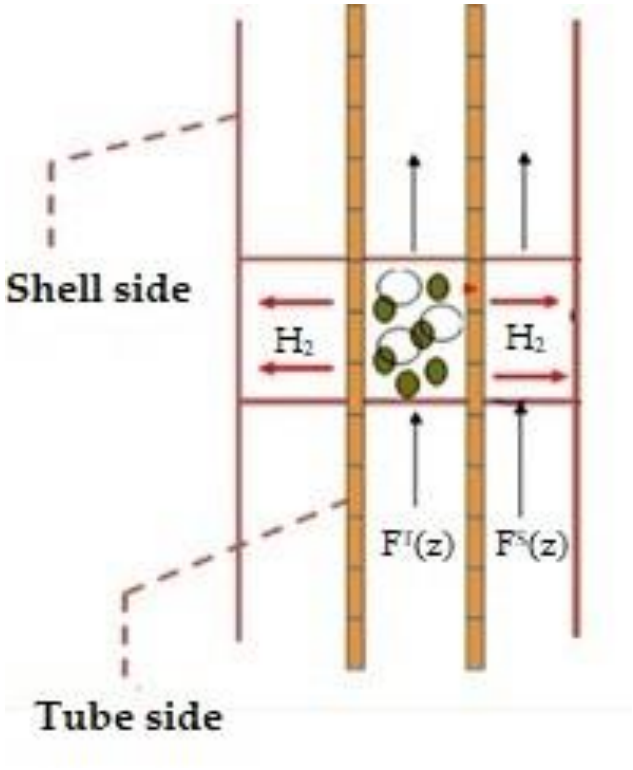

Figure 2.7: FBMR proposed model

2.6 Permeation via dense palladium membrane

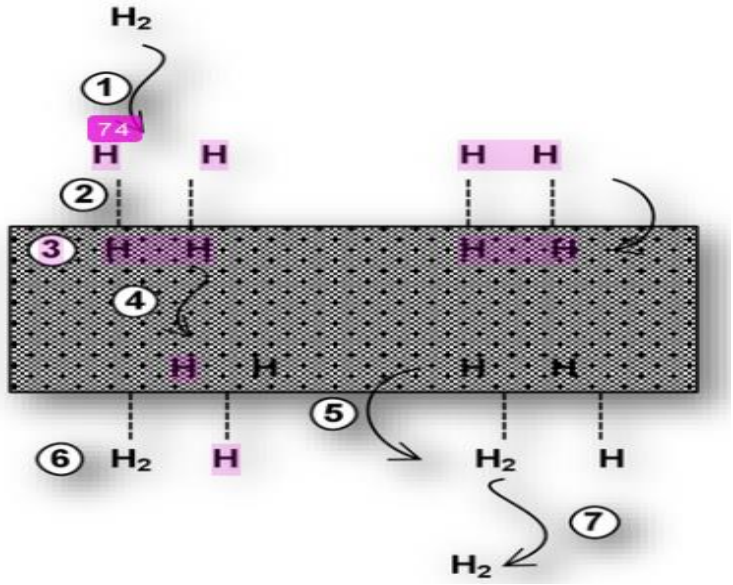

Figure 2.8: Hydrogen permeation from walls [33]

The membrane material of choice is a palladium-silver alloy combining the excellent perm selectivity of palladium with silver providing mechanical stability. Hydrogen gas in the product permeates through the membrane surface, which results in displacement of equilibrium in the forward direction and thus both reformate and hydrogen yield is increased. Hydrogen gas permeation through a dense membrane is explained via the solution diffusion model. The hydrogen gas molecules are split into atoms and diffuse through the palladium metal alloy. On the other side the atoms are again recombined into atoms and pass into the sweep gas. The hydrogen permeation process is shown in Figure 2.8.

Inside the shell it can be a vacuum or hydrogen as sweep gas the pressure of which is a controlled variable to control the driving force for hydrogen permeation. In this simulation the thickness of the membrane is taken to be 10 mm. A stainless steel support carries the Pd–Ag (23% Ag) membrane. Membrane length is equal to 6.29 m and its area is 30.02 m^2.

Chapter-3

Literature Review

Two reference works deserve special mention for providing a head start with valuable information on the industrial practice of naphtha reforming. One of the two books is a text dedicated exclusively to the subject of catalytic naphtha reforming, Aitani (2004) [1]. The second book, by Ancheyta (2011) provided an in depth review of the current state of the art in modelling and simulation of the naphtha reforming process [2]. A number of other references were also obtained to learn more about different types of catalytic reformers operated for naphtha reforming.

A complex process such as naphtha reforming necessitates the development of a simulation model that can help in understanding for engineers and a tool for operator training and optimizing the process. A lot of research has been carried out on various aspects of the reforming process by a number of researchers. Naphtha is a complex mixture of more than a hundred compounds thus the first task is to resolve this mixture into identifiable compounds which is then be used to model the actual process. Researchers have tackled this issue by representing various 'lumps' of compounds by a single pseudo-component that has average properties of that lump. This way the number of compounds and reactions can be reduced to a workable number. These lumped components are then described to undergo various reforming reactions.

Different researchers have presented kinetic models of varying complexity for representing naphtha catalytic reforming. It is now 50 years back when kinetic delumping of naphtha was attempted. One of the very first kinetic model is one proposed by Smith in 1959 [24]. Smith's study revealed that naphtha is in fact a mixture of three distinct hydrocarbon classes. No further classification was attempted. Researchers using Smith's model assume that a single compound in each category will be able to represent the complete class. Further work by Krane (1959) extended the number of compounds within each major category and worked with 20 representative components [36]. Hydrocarbons up to 10 carbon atoms were considered to compose whole naphtha, with emphasis on difference

between paraffins, naphthenes, and aromatics within each carbon number group. Krane's network is composed of 53 total reaction steps. Lee et al. (1997) utilized Smith's kinetic model to model a continuous catalyst regeneration type catalytic naphtha reformer with the target of obtaining optimal conditions for an industrial operation [38, 39]. Kmak developed a detailed model (Exxon model) and considers twenty-two lumps [37]. This model was later refined by Froment that considers twenty-eight lumps in the model undergoing 81 reactions [25]. All these models presented the naphtha feed as mixture of pseudo components which are not suitable to be adopted by Aspen PLUS environment. Aspen PLUS requires that actual compounds be taken from its vast database.

A suitable model was presented by Padmavathi together with improvements by Iranshahi et al. [31, 32]. This model was chosen because of its published reaction rate data. The reactions have been categorized in dehydrogenation, dehydrocyclization, isomerization, transalkylation, hydrocracking, and hydrodealkylation types.

Process design intensively involves process simulators such as Aspen HYSYS/PLUS, CHEMCAD, etc. Various researchers have used platforms such as MATLAB and other ODE solvers to simulate naphtha reforming operation. Outside of academia there is not much choice of software for process engineers due to high cost of commercial packages. Aspen PLUS is the platform of choice due to its extensive database of pure components and built-in modules for simulating a wide array of unit operations.

Fazeli simulated a network of three adiabatic naphtha reforming reactors using MATLAB [35]. Kinetic network of Padmavathi was used to simulate data from a local refinery of Tehran.HOU Weifang utilized the Aspen PLUS platform and developed a complete model of a naphtha reforming unit using an 18-lump kinetic model [30]. Kinetics were implemented using a separate user module and optimization studies were carried out.
Mostafazadeh presented the concept of PBMR and Rahimpour developed an FBMR [15, 16]. Reaction scheme of smith was used in both studies and material balance equations were solved using backward finite difference. The insertion of palladium-based membrane improved the aromatic and hydrogen production rate in both cases.

As the Aspen PLUS environment lacks an intrinsic model for simulating a fluidized bed membrane reactor, various researchers have tried combinations of built-in ideal reactors to mimic the complex hydrodynamics inside a fluidized bed.

Rosario et al modeled the reactor system for chemical looping combustion using PFR and CSTR pairs [34]. They divided the reactor working in bubbling regime into 5 CSTR pairs to represent hydrodynamics inside the fluidized bed reactor. Sarvar-Amini validated the results of Adris for steam reforming of methane by constructing an Aspen PLUS based FBMR [19]. FBMR was represented using pairs of CSTR and PFR and calculator blocks were used for calculation of hydrodynamic parameters and membrane permeation phenomena.

Genyin Ye et al modeled the steam reforming process on Aspen PLUS platform by axially dividing an FBMR into pairs of Gibbs reactor and a membrane module [20]. Membrane permeation was implemented by using external FORTRAN subroutine. Pasha modeled the SMR reaction on the steps of Genyin but instead used Excel interfacing to implement membrane permeation phenomena [33].

From the above discussion it is evident that there has been no study conducted on the simulation of the FBMR for the naphtha reforming process in the Aspen PLUS environment.

3.1 Objectives

Aspen PLUS is an industry leading software in terms of process design and is frequently the program of choice for carrying out simulation and optimization studies. As of this writing a fluidized bed membrane reactor is not available in the Aspen PLUS environment so a customized approach is followed.

The first task as evident from the objectives of this study was to prepare an Aspen PLUS model of a catalytic naphtha reformer, detailed enough to represent the actual process characteristics reasonably well. In this study, the naphtha reforming process is modeled in the Aspen PLUS environment. The fluidized bed reactor is represented by combining the

ideal CSTR and PFR modules available inside Aspen PLUS. Membrane separation process is incorporated through Excel interfacing.

The following steps were systematically followed to achieve the objective:

- Modeling of the catalytic naphtha reforming process occurring in a fluidized bed reactor in the Aspen PLUS environment.
- Implement the hydrodynamic process occurring inside the fluidized-bed using CSTR and PFR modules available in the Aspen PLUS environment.
- Convert the model of FBR into FBMR via addition of membrane permeation using external Excel file through which Sievert's equation implemented.
- Compare results from both of the reactors to study the benefits derived from the addition of membrane.

Chapter-4

Model Development

A fluidized bed being a non-ideal reactor such that its hydrodynamics cannot be simply assumed to be that of a plug flow type or of a perfectly mixed one. Two distinct phases are identified in a fluidized bed: emulsion phase and bubble phase. An Excel file is developed for the calculation of the hydrodynamic parameters using the two-phase theory of fluidization. This Excel block calculates the flow distribution, and the volumes of CSTR and PFR. Another Excel file implements the Sievert's equation to simulate the phenomena of membrane permeation

Preliminary Assumptions:

Two distinct phases are identified in a fluidized bed: a dense phase and a lean phase composed of gas bubbles. The following is assumed for development of the model:

- Steady-state and pseudo-steady-state operation;
- Much of the reactions occur within the emulsion phase;
- Permeation of hydrogen occurs from emulsion phase only;
- Hydrogen diffuses through the membrane radially;
- Assumption of spherical bubbles hold;
- Movement of gas in bubbles is assumed to follow plug flow and due to very low quantity of catalyst the reaction rates are very low compared to emulsion phase gas;
- Contents of the bed are well mixed and both emulsion and bubble phase are at a uniform temperature;
- Adiabatic conditions;
- The membrane is 100% perm-selective for hydrogen;
- Sieverts' law is applicable for hydrogen permeation through the membrane.

The following two sub-sections describe the membrane integration within Aspen PLUS and the combination of CSTR and PFR reactor with the membrane module to simulate the overall FBMR process.

4.1 Simulating the phenomena of fluidization in Aspen PLUS

A fluidized bed exhibits complex hydrodynamics. To model its behavior, the dense bed is divided into bubble phase and an emulsion phase. Membrane permeation occurs simultaneously with the reaction. An Excel file is developed which calculates the hydrodynamic parameters of the fluidized bed. The equations used from the literature are presented in Table 4.1. The output from this file is transferred to the CSTR and PFR units through an internal Excel interface and transfer modules.

Gas flowing in the form of bubbles is modelled as flowing through a plug flow reactor and the gas flowing though the emulsion phase is modelled as flowing through a mixed flow reactor or a CSTR. In this way the fluidized bed reactor is represented by PFR and CSTR which are available as standard modules in the Aspen PLUS environment. A separate 'SPLT' Excel file is used to implement equations described in Table 4.1.

After evaluating the hydrodynamic parameters, the data is transferred to Aspen PLUS which uses its internal database to calculate thermodynamic properties based on material and energy balance equations. The effluent streams from each section is then transferred to the 'TRF' Excel block where both effluent streams are mixed and in addition the Sievert's equation in the case of the FBMR is implemented. Afterwards the exit streams are transferred to respective PFR and CSTR for the next section (i+1). Calculations then proceed in this manner until they reach the top most section of the bed.

Table 4.1: Hydrodynamic parameters [33-35]

Parameter	Equation
Superficial velocity at minimum fluidization	$\frac{1.75}{\epsilon_{mf}^3 \varphi_s}\left[\frac{d_p \rho_g u_{mf}}{\mu}\right]^2 + \frac{150(1-\epsilon_{mf})}{\epsilon_{mf}^3 \varphi_s}\left[\frac{d_p \rho_g u_{mf}}{\mu}\right]$
Archimedes' number	$Ar = \frac{d_p^3 \rho_g (\rho_p - \rho_g) g}{\mu^2}$
Bubble diameter	$d_b = d_{bm}(d_{bm} - d_{b0})exp(-0.3z/D)$
	$d_{b0} = 0.376(u_0 - u_{mf})^2$
	$d_{bm} = 0.65\left[\frac{\pi}{4}D^2(u_0 - u_{mf})\right]^{0.4}$
Coefficient for mass transfer from bubble to emulsion phase	$K_{be} = \frac{u_{mf}}{3}\left[\left(4D_{jm}\epsilon_{mf}u_b/(\pi d_b)\right)\right]^{1/2}$
Velocity of bubble rise	$u_b = u - u_{mf} + 0.711\sqrt{g d_b}$
Volume fraction of bubble phase to overall bed	$\delta = (u - u_{mf})/u_b$
Specific surface area for bubble	$a_b = 6\delta/d_b$
Density for emulsion phase	$\rho_e = \rho_p(1 - \epsilon_{mf})$

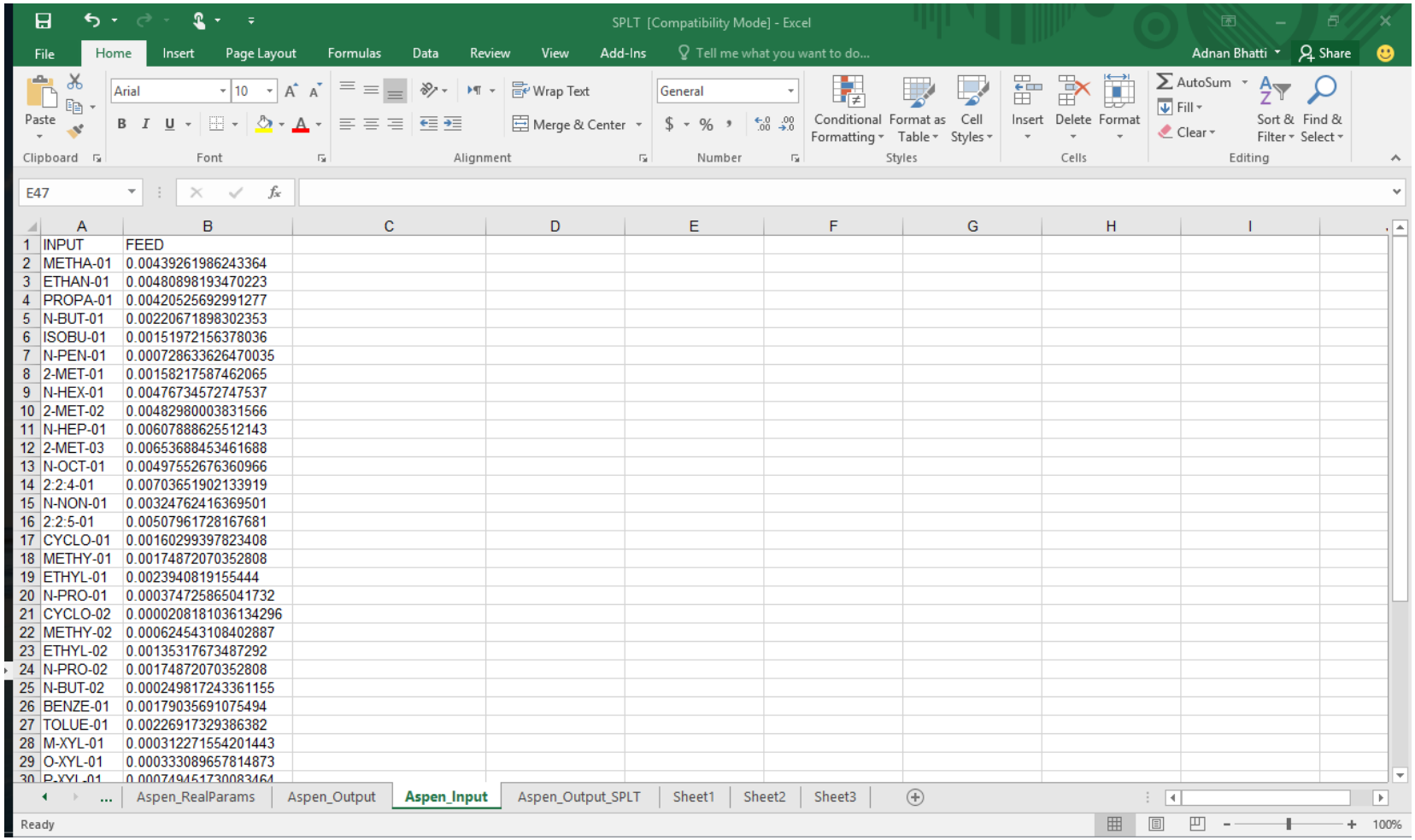

	A	B	C	D	E	F	G	H	I
1	INPUT	FEED							
2	METHA-01	0.00439261986243364							
3	ETHAN-01	0.00480898193470223							
4	PROPA-01	0.00420525692991277							
5	N-BUT-01	0.00220671898302353							
6	ISOBU-01	0.00151972156378036							
7	N-PEN-01	0.000728633626470035							
8	2-MET-01	0.00158217587462065							
9	N-HEX-01	0.00476734572747537							
10	2-MET-02	0.00482980003831566							
11	N-HEP-01	0.00607888625512143							
12	2-MET-03	0.00653688453461688							
13	N-OCT-01	0.00497552676360966							
14	2:2:4-01	0.00703651902133919							
15	N-NON-01	0.00324762416369501							
16	2:2:5-01	0.00507961728167681							
17	CYCLO-01	0.00160299397823408							
18	METHY-01	0.00174872070352808							
19	ETHYL-01	0.0023940819155444							
20	N-PRO-01	0.000374725865041732							
21	CYCLO-02	0.0000208181036134296							
22	METHY-02	0.000624543108402887							
23	ETHYL-02	0.00135317673487292							
24	N-PRO-02	0.00174872070352808							
25	N-BUT-02	0.000249817243361155							
26	BENZE-01	0.00179035691075494							
27	TOLUE-01	0.00226917329386382							
28	M-XYL-01	0.000312271554201443							
29	O-XYL-01	0.000333089657814873							
30	P-XYL-01	0.000749451730083464							

Figure 4.1: Aspen input sheet in Excel for SPLT

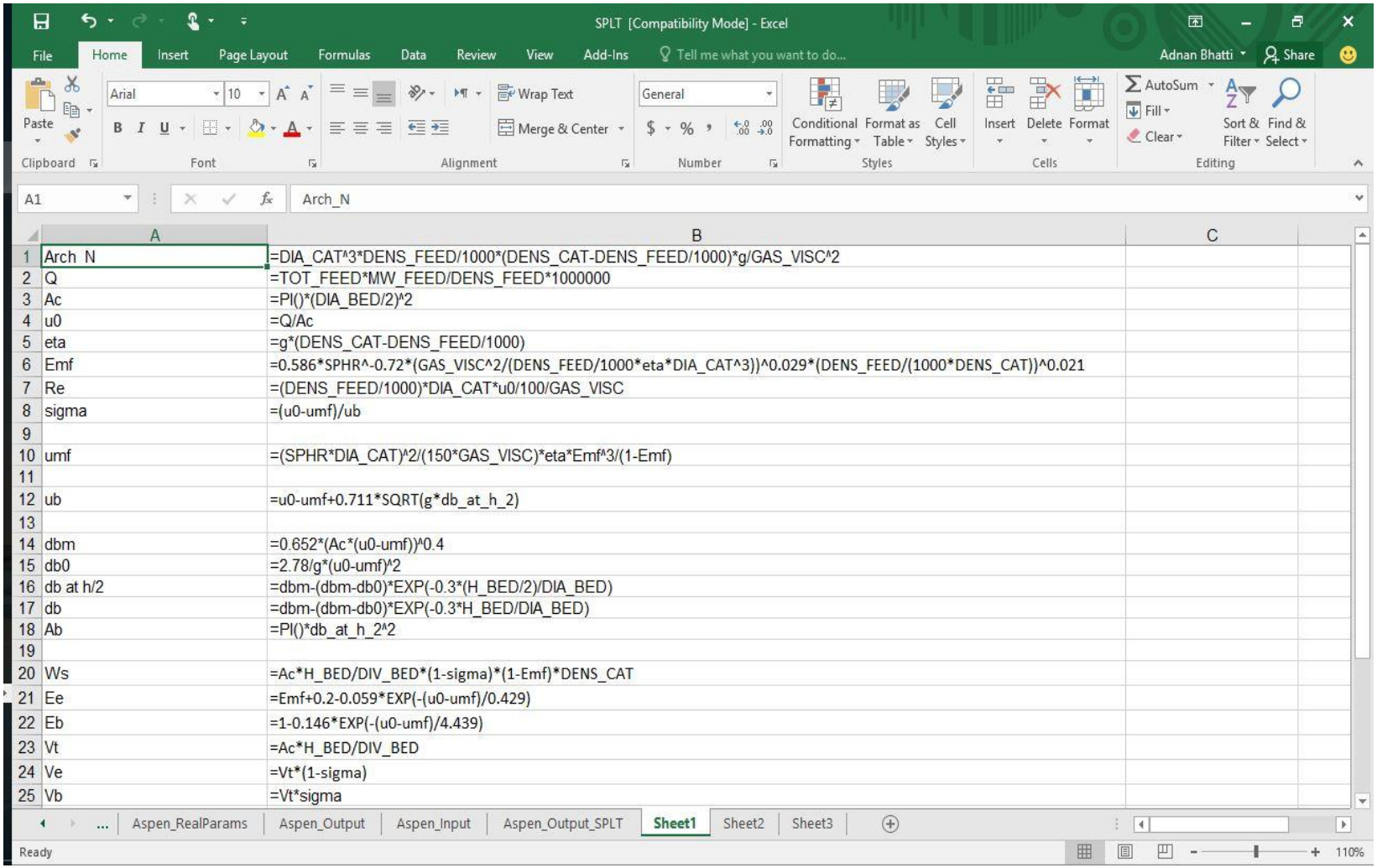

Figure 4.2: Equations sheet in Excel for SPLT block in Aspen PLUS

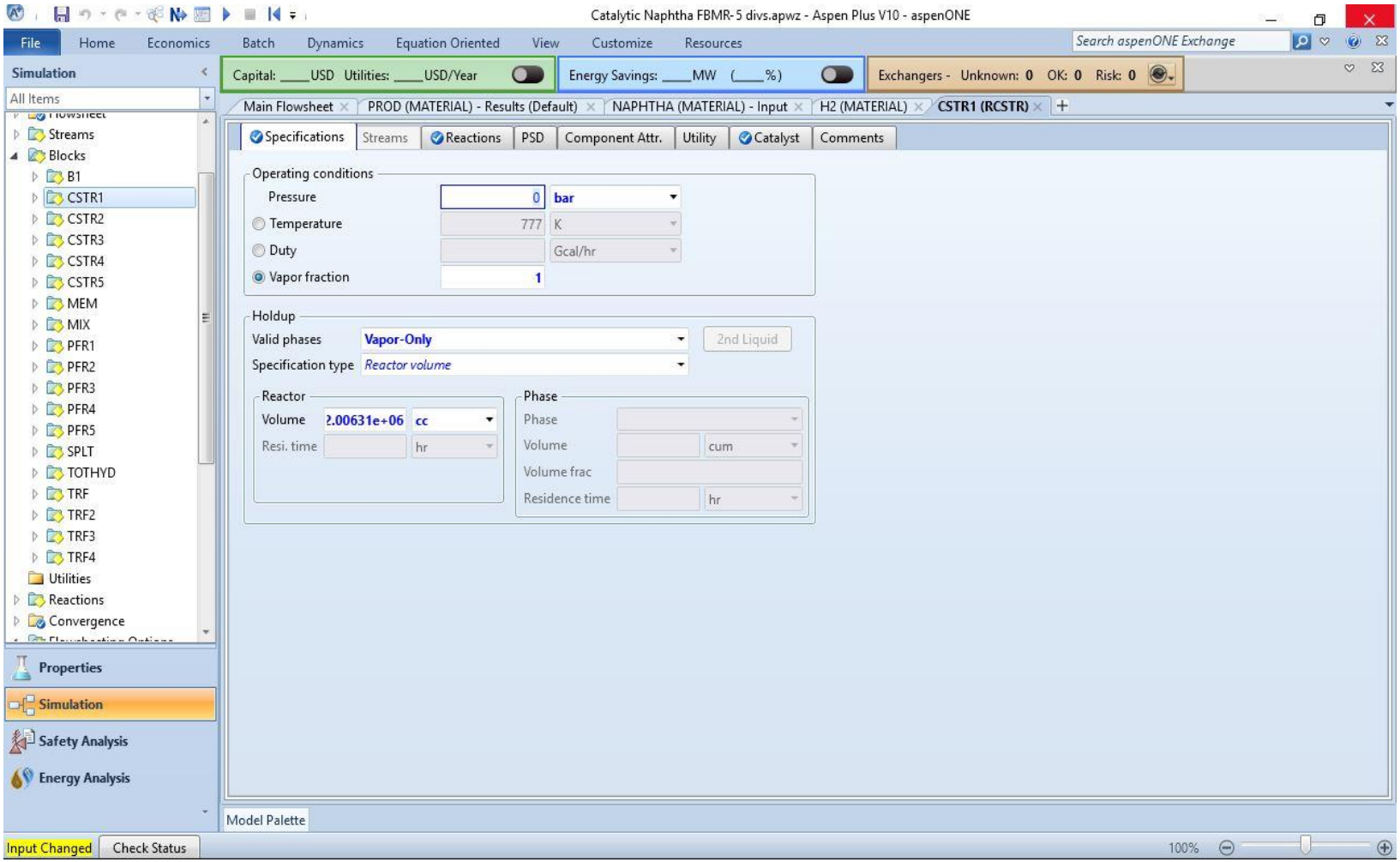

Figure 4.3: CSTR input sheet in Aspen PLUS

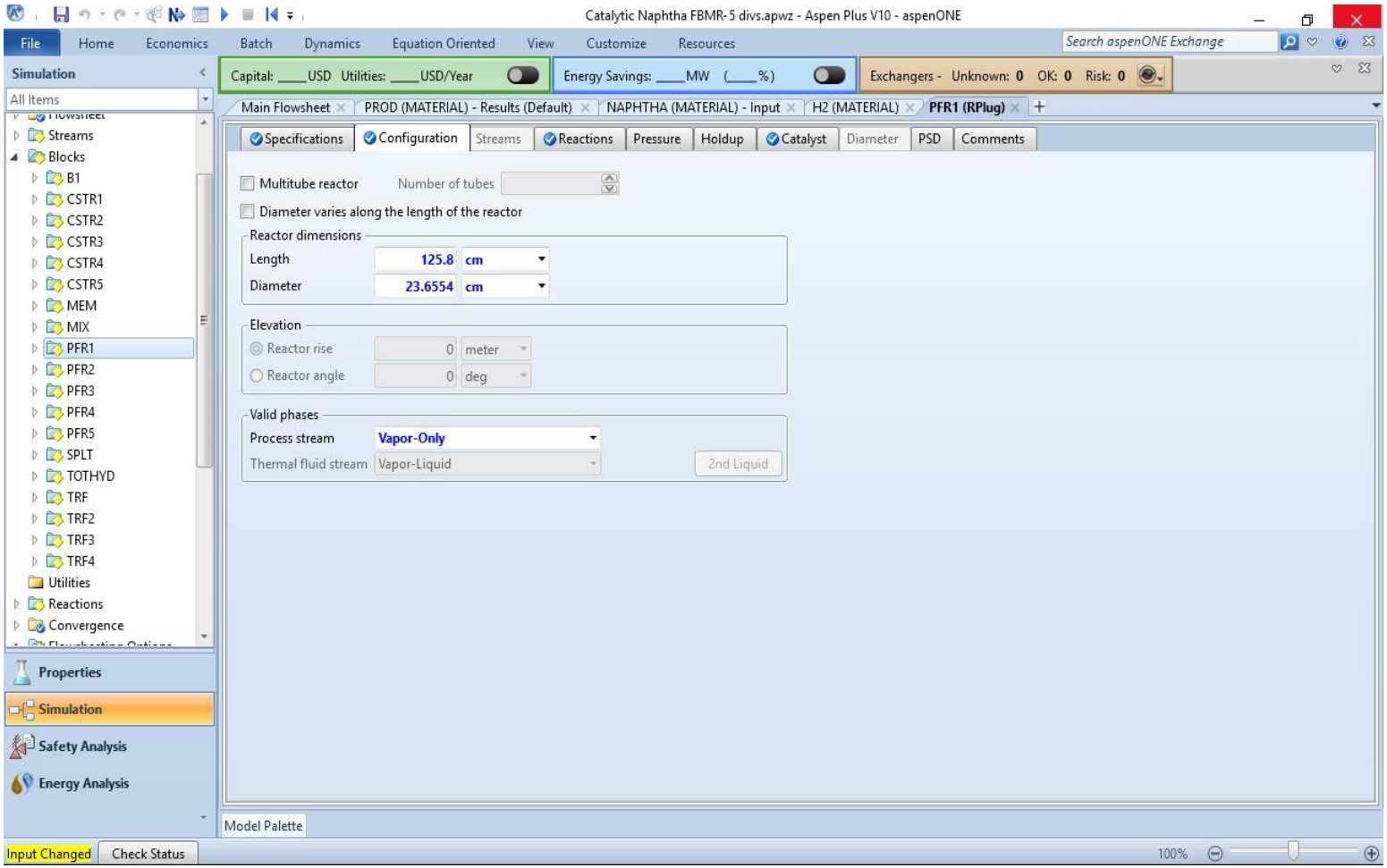

Figure 4.4: PFR input sheet in Aspen PLUS

4.2 Membrane permeation

The membrane performance is affected by non-uniformity in membrane fabrication, blockage of the membrane surface by catalyst dust etc. The membrane permeation effectiveness factor (η) account for all these negative influences on permeation rate and determined experimentally [15]. To simulate the hydrogen permeation process through the membrane tube, User a Model 2-unit operation block with an Excel spreadsheet was used to perform the calculations. Aspen PLUS supplies properties of the feed stream of the user model and some additional parameters ($\eta, k, C_{mp}, E, R, T, P_{RH_2}$ and P_{MH_2}) to the Excel spreadsheet. Excel organizes this information and calculates product stream properties with hydrogen production rate (Q_{H_2}) based on Sieverts' law, Equation 4.1. This information is then returned to the Aspen PLUS interface and results are displayed.

$$Q_{H_2} = \eta k C_{mp}\left[P_{RH_2}^{0.5} - P_{MH_2}^{0.5}\right]e^{\left(-\frac{E_a}{RT}\right)} \text{----------(4.1)}$$

.

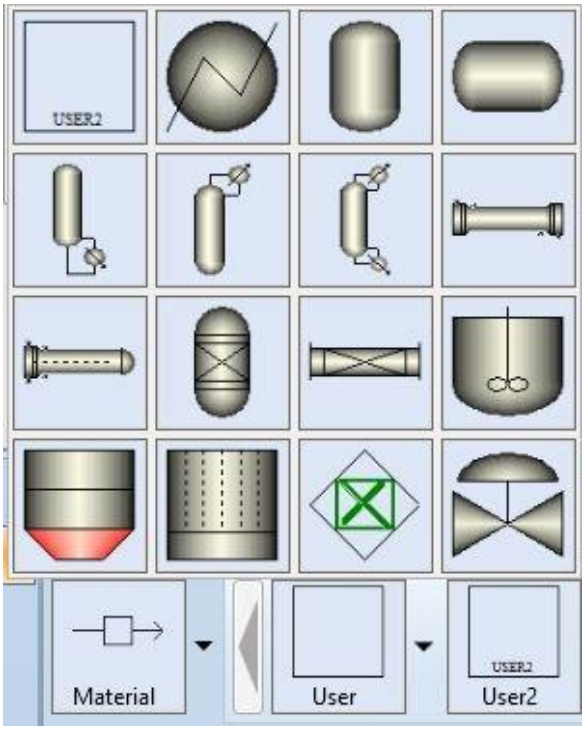

Figure 4.5: User 2 custom model selection pane in Aspen PLUS

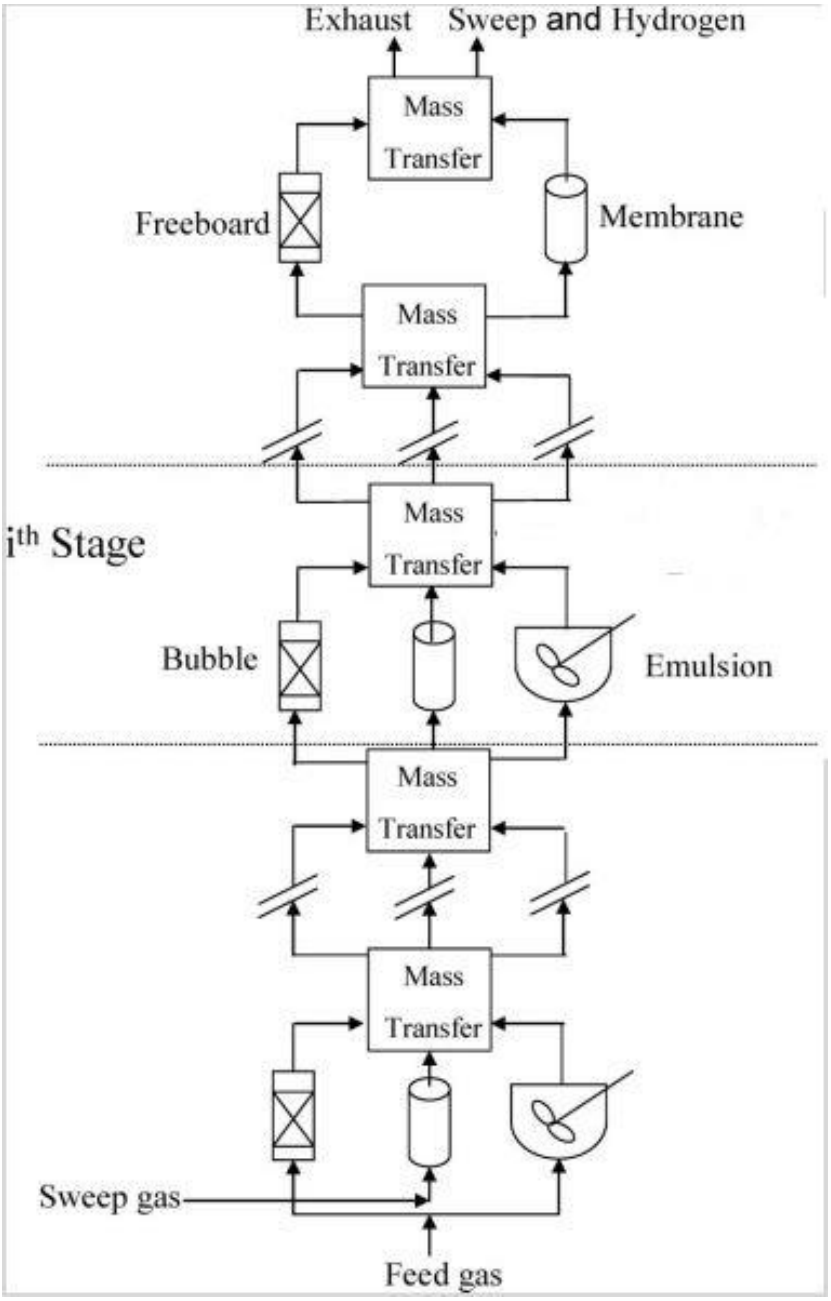

Figure 4.6: Sequential modular scheme for simulation of FBMR in Aspen PLUS [19]

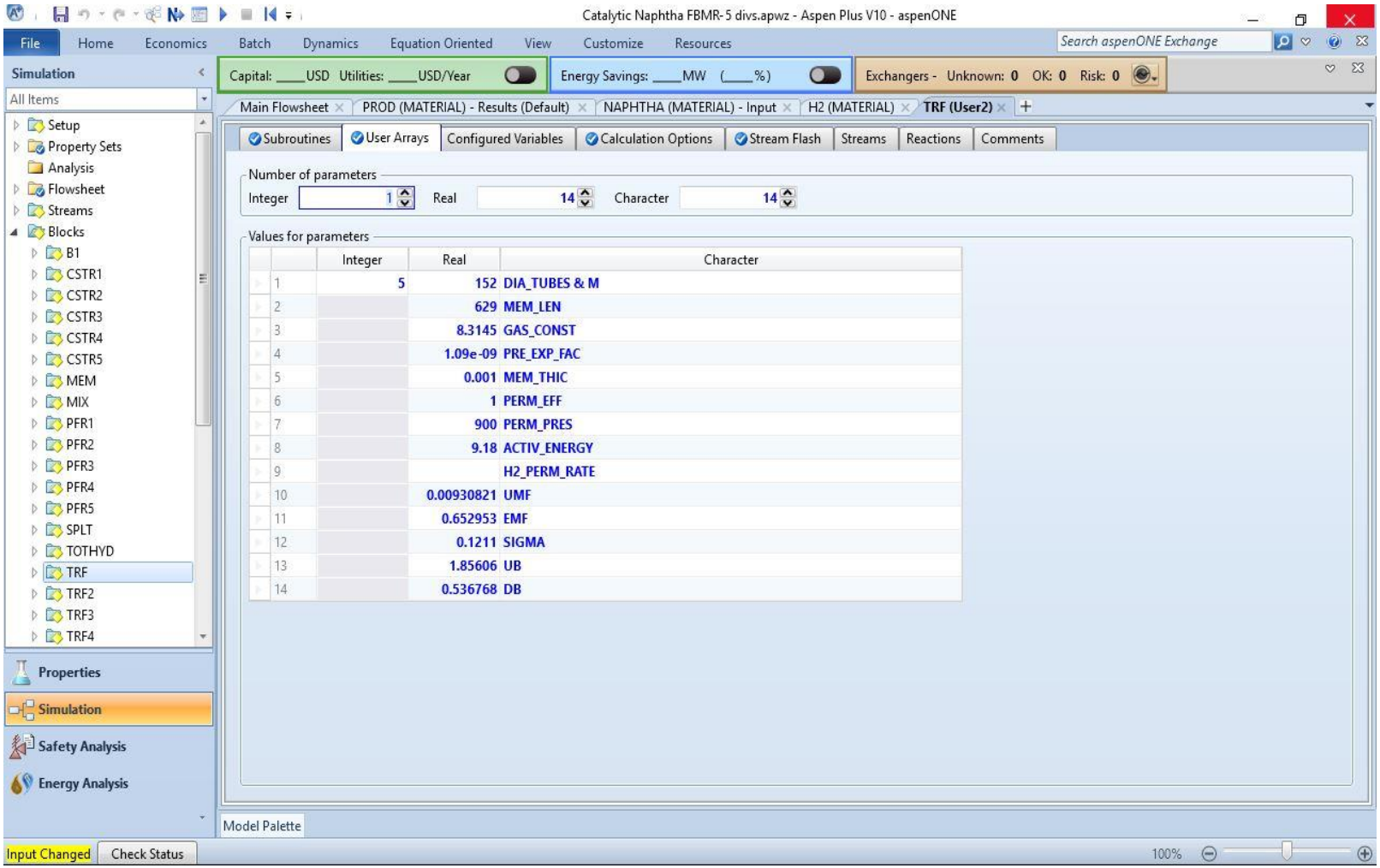

Figure 4.7: Mass Transfer input pane for User 2 model in Aspen PLUS

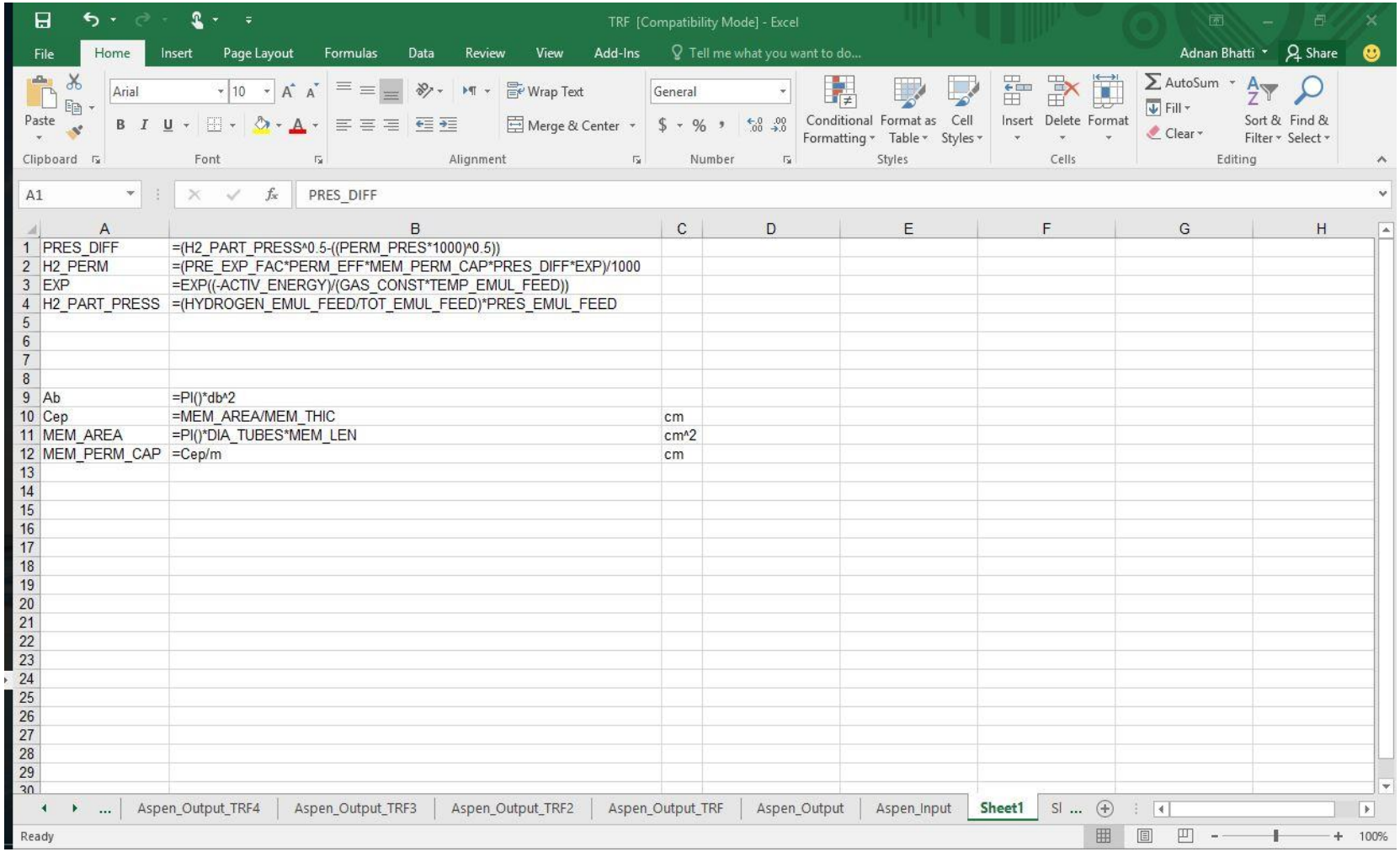

Figure 4.8: Equations sheet in Excel for TRF block in Aspen PLUS

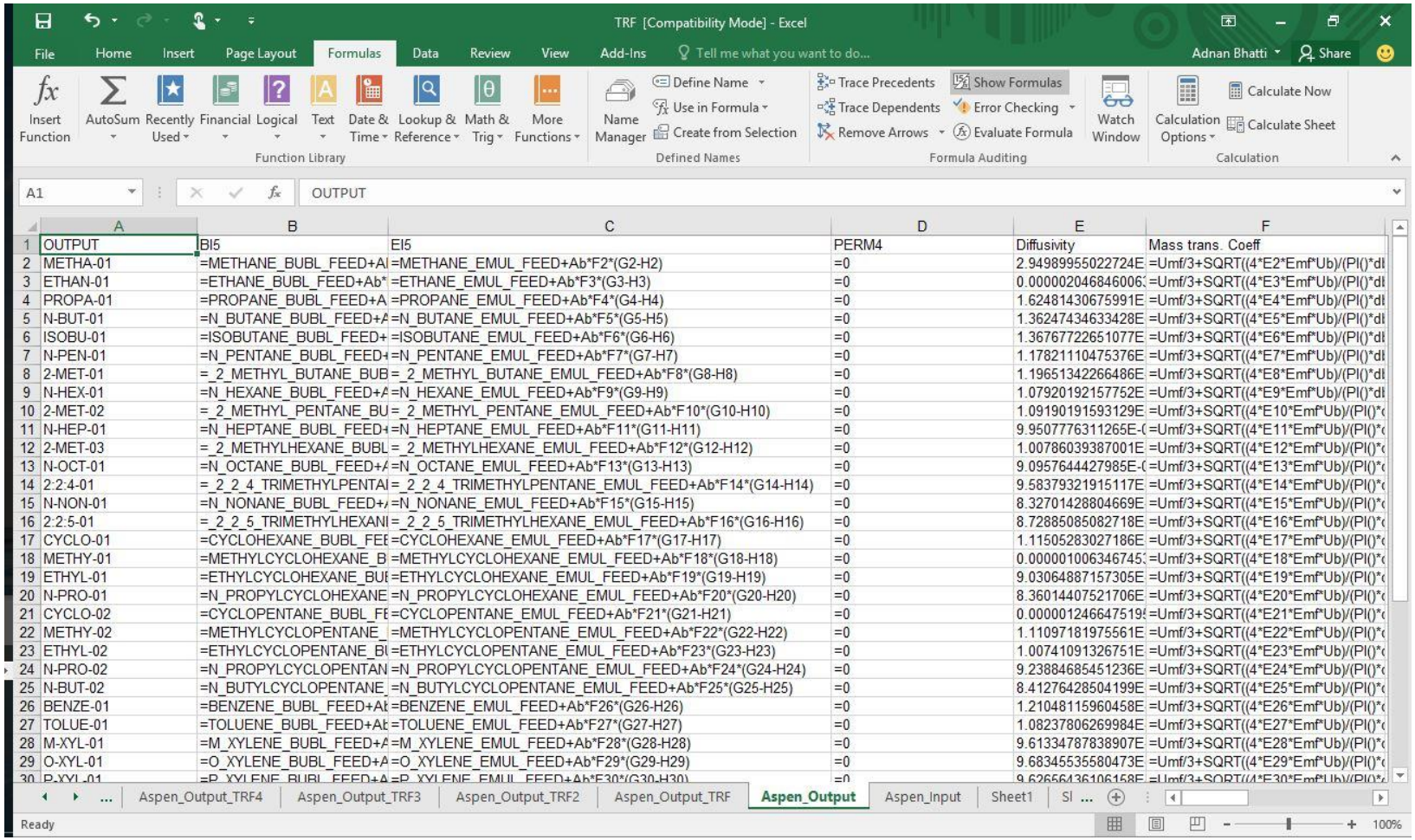

	A	B	C	D	E	F
1	OUTPUT	BI5	EI5	PERM4	Diffusivity	Mass trans. Coeff
2	METHA-01	=METHANE_BUBL_FEED+AI	=METHANE_EMUL_FEED+Ab*F2*(G2-H2)	=0	2.94989955022724E	=Umf/3+SQRT((4*E2*Emf*Ub)/(PI()*dI
3	ETHAN-01	=ETHANE_BUBL_FEED+Ab*	=ETHANE_EMUL_FEED+Ab*F3*(G3-H3)	=0	0.000002046846006	=Umf/3+SQRT((4*E3*Emf*Ub)/(PI()*dI
4	PROPA-01	=PROPANE_BUBL_FEED+A	=PROPANE_EMUL_FEED+Ab*F4*(G4-H4)	=0	1.62481430675991E	=Umf/3+SQRT((4*E4*Emf*Ub)/(PI()*dI
5	N-BUT-01	=N_BUTANE_BUBL_FEED+A	=N_BUTANE_EMUL_FEED+Ab*F5*(G5-H5)	=0	1.36247434633428E	=Umf/3+SQRT((4*E5*Emf*Ub)/(PI()*dI
6	ISOBU-01	=ISOBUTANE_BUBL_FEED+	=ISOBUTANE_EMUL_FEED+Ab*F6*(G6-H6)	=0	1.36767722651077E	=Umf/3+SQRT((4*E6*Emf*Ub)/(PI()*dI
7	N-PEN-01	=N_PENTANE_BUBL_FEED+	=N_PENTANE_EMUL_FEED+Ab*F7*(G7-H7)	=0	1.17821110475376E	=Umf/3+SQRT((4*E7*Emf*Ub)/(PI()*dI
8	2-MET-01	=_2_METHYL_BUTANE_BUB	=_2_METHYL_BUTANE_EMUL_FEED+Ab*F8*(G8-H8)	=0	1.19651342266486E	=Umf/3+SQRT((4*E8*Emf*Ub)/(PI()*dI
9	N-HEX-01	=N_HEXANE_BUBL_FEED+A	=N_HEXANE_EMUL_FEED+Ab*F9*(G9-H9)	=0	1.07920192157752E	=Umf/3+SQRT((4*E9*Emf*Ub)/(PI()*dI
10	2-MET-02	=_2_METHYL_PENTANE_BU	=_2_METHYL_PENTANE_EMUL_FEED+Ab*F10*(G10-H10)	=0	1.09190191593129E	=Umf/3+SQRT((4*E10*Emf*Ub)/(PI()*(
11	N-HEP-01	=N_HEPTANE_BUBL_FEED+	=N_HEPTANE_EMUL_FEED+Ab*F11*(G11-H11)	=0	9.9507776311265E-(	=Umf/3+SQRT((4*E11*Emf*Ub)/(PI()*(
12	2-MET-03	=_2_METHYLHEXANE_BUBL	=_2_METHYLHEXANE_EMUL_FEED+Ab*F12*(G12-H12)	=0	1.00786039387001E	=Umf/3+SQRT((4*E12*Emf*Ub)/(PI()*(
13	N-OCT-01	=N_OCTANE_BUBL_FEED+A	=N_OCTANE_EMUL_FEED+Ab*F13*(G13-H13)	=0	9.0957644427985E-(	=Umf/3+SQRT((4*E13*Emf*Ub)/(PI()*(
14	2:2:4-01	=_2_2_4_TRIMETHYLPENTAI	=_2_2_4_TRIMETHYLPENTANE_EMUL_FEED+Ab*F14*(G14-H14)	=0	9.58379321915117E	=Umf/3+SQRT((4*E14*Emf*Ub)/(PI()*(
15	N-NON-01	=N_NONANE_BUBL_FEED+A	=N_NONANE_EMUL_FEED+Ab*F15*(G15-H15)	=0	8.32701428804669E	=Umf/3+SQRT((4*E15*Emf*Ub)/(PI()*(
16	2:2:5-01	=_2_2_5_TRIMETHYLHEXANI	=_2_2_5_TRIMETHYLHEXANE_EMUL_FEED+Ab*F16*(G16-H16)	=0	8.72885085082718E	=Umf/3+SQRT((4*E16*Emf*Ub)/(PI()*(
17	CYCLO-01	=CYCLOHEXANE_BUBL_FEE	=CYCLOHEXANE_EMUL_FEED+Ab*F17*(G17-H17)	=0	1.11505283027186E	=Umf/3+SQRT((4*E17*Emf*Ub)/(PI()*(
18	METHY-01	=METHYLCYCLOHEXANE_B	=METHYLCYCLOHEXANE_EMUL_FEED+Ab*F18*(G18-H18)	=0	0.000001006346745	=Umf/3+SQRT((4*E18*Emf*Ub)/(PI()*(
19	ETHYL-01	=ETHYLCYCLOHEXANE_BUI	=ETHYLCYCLOHEXANE_EMUL_FEED+Ab*F19*(G19-H19)	=0	9.03064887157305E	=Umf/3+SQRT((4*E19*Emf*Ub)/(PI()*(
20	N-PRO-01	=N_PROPYLCYCLOHEXANE	=N_PROPYLCYCLOHEXANE_EMUL_FEED+Ab*F20*(G20-H20)	=0	8.36014407521706E	=Umf/3+SQRT((4*E20*Emf*Ub)/(PI()*(
21	CYCLO-02	=CYCLOPENTANE_BUBL_FE	=CYCLOPENTANE_EMUL_FEED+Ab*F21*(G21-H21)	=0	0.000001246647519	=Umf/3+SQRT((4*E21*Emf*Ub)/(PI()*(
22	METHY-02	=METHYLCYCLOPENTANE_	=METHYLCYCLOPENTANE_EMUL_FEED+Ab*F22*(G22-H22)	=0	1.11097181975561E	=Umf/3+SQRT((4*E22*Emf*Ub)/(PI()*(
23	ETHYL-02	=ETHYLCYCLOPENTANE_BU	=ETHYLCYCLOPENTANE_EMUL_FEED+Ab*F23*(G23-H23)	=0	1.00741091326751E	=Umf/3+SQRT((4*E23*Emf*Ub)/(PI()*(
24	N-PRO-02	=N_PROPYLCYCLOPENTAN	=N_PROPYLCYCLOPENTANE_EMUL_FEED+Ab*F24*(G24-H24)	=0	9.23884685451236E	=Umf/3+SQRT((4*E24*Emf*Ub)/(PI()*(
25	N-BUT-02	=N_BUTYLCYCLOPENTANE_	=N_BUTYLCYCLOPENTANE_EMUL_FEED+Ab*F25*(G25-H25)	=0	8.41276428504199E	=Umf/3+SQRT((4*E25*Emf*Ub)/(PI()*(
26	BENZE-01	=BENZENE_BUBL_FEED+Ab	=BENZENE_EMUL_FEED+Ab*F26*(G26-H26)	=0	1.21048115960458E	=Umf/3+SQRT((4*E26*Emf*Ub)/(PI()*(
27	TOLUE-01	=TOLUENE_BUBL_FEED+Ab	=TOLUENE_EMUL_FEED+Ab*F27*(G27-H27)	=0	1.08237806269984E	=Umf/3+SQRT((4*E27*Emf*Ub)/(PI()*(
28	M-XYL-01	=M_XYLENE_BUBL_FEED+A	=M_XYLENE_EMUL_FEED+Ab*F28*(G28-H28)	=0	9.61334787838907E	=Umf/3+SQRT((4*E28*Emf*Ub)/(PI()*(
29	O-XYL-01	=O_XYLENE_BUBL_FEED+A	=O_XYLENE_EMUL_FEED+Ab*F29*(G29-H29)	=0	9.68345535580473E	=Umf/3+SQRT((4*E29*Emf*Ub)/(PI()*(
30	P-XYL-01	=P_XYLENE_BUBL_FEED+A	=P_XYLENE_EMUL_FEED+Ab*F30*(G30-H30)	=0	9.62666436106168E	=Umf/3+SQRT((4*E30*Emf*Ub)/(PI()*(

Figure 4.9: Aspen Output sheet in Excel for TRF block in Aspen PLUS

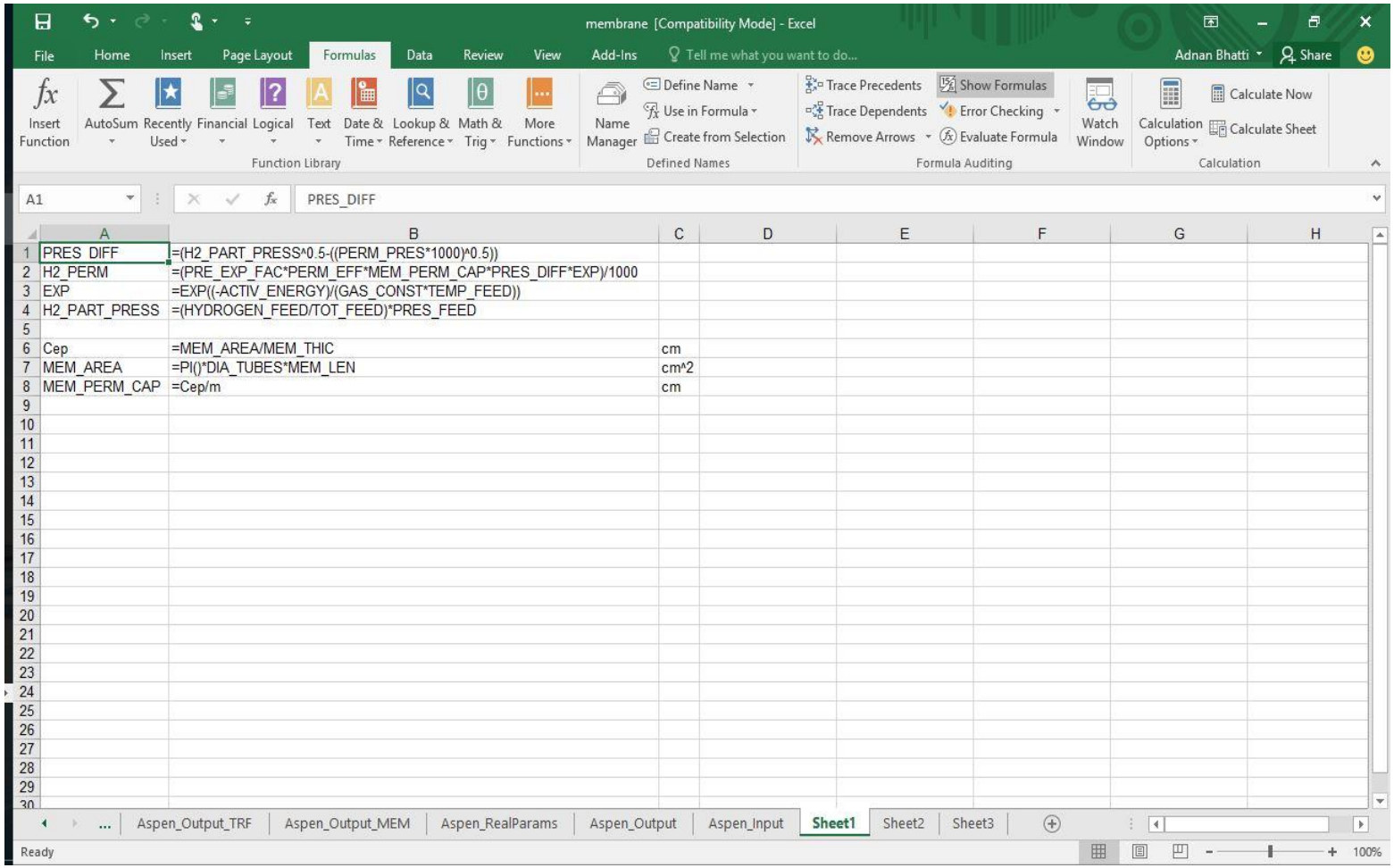

Figure 4.10: Equations sheet in Excel for simple membrane permeation block in Aspen PLUS

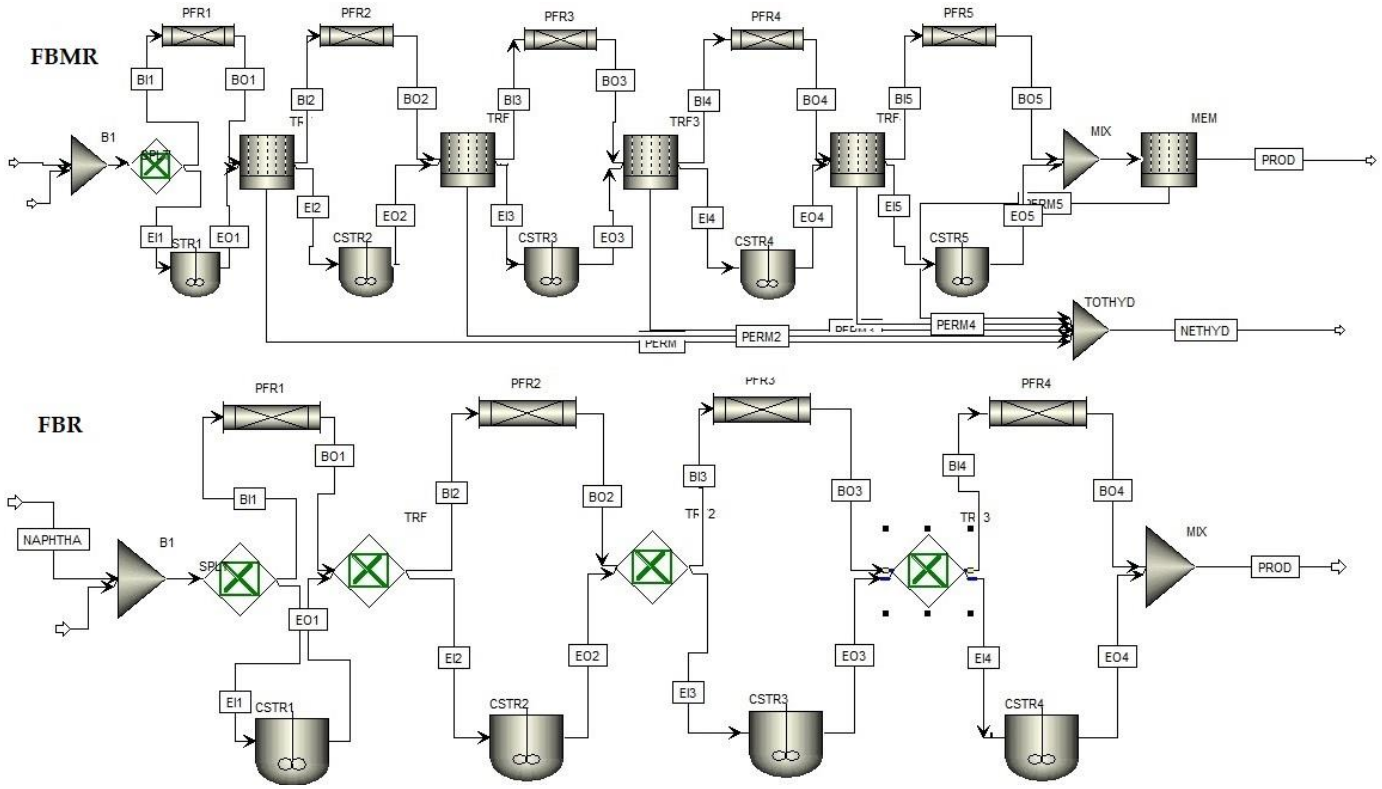

Figure 4.11: ASPEN Plus flowsheet for FBMR and FBR

4.3 Determination of number of stages

The effect of increasing the number of stages is that there is an increase in the transfer of partially reacted bubble gas to emulsion gas where it will have higher chances for reaction. The right number of stages to model this system is dependent on its kinetics and hydrodynamics.

The reformer is divided into 4-5 sections to simulate the environment inside a real world reforming unit. Figure 4.12 shows that as the number of sections are increased the rate of increase (or decrease in the case of naphthenes) of hydrogen decreases thus the production (or consumption) becomes steady. A further increase in subsections alters the hydrodynamics from that of a CSTR to that inside a PFR. For the FBMR the number of stages was determined to be 5. For comparison, FBR with no membrane permeation was simulated and similarly, the number of optimal stages were found to be 4.

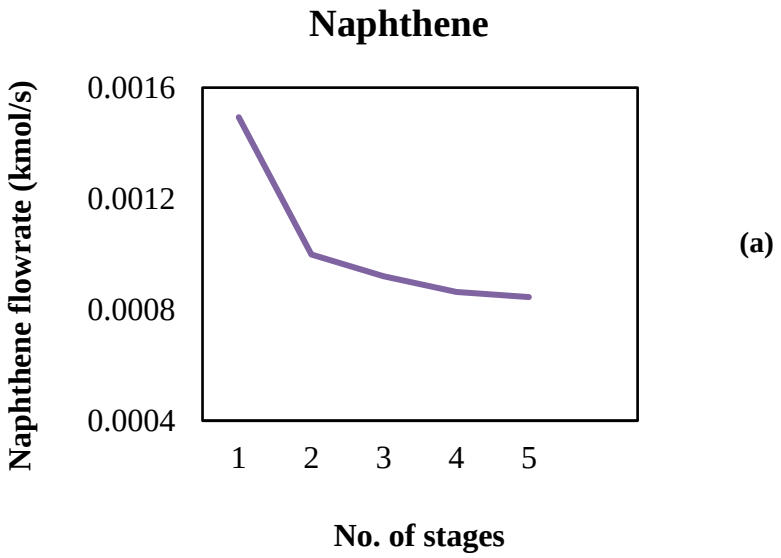

Figure 4.12: Effect of number of stages on FBMR (a) Naphthene flowrate

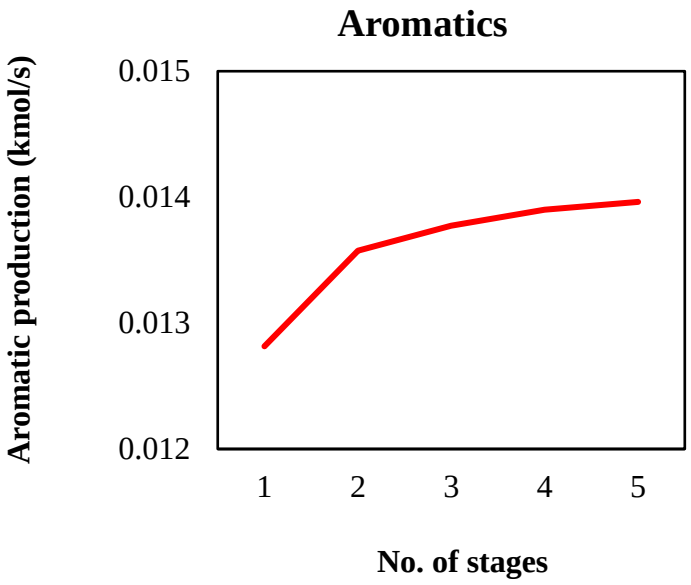

(b)

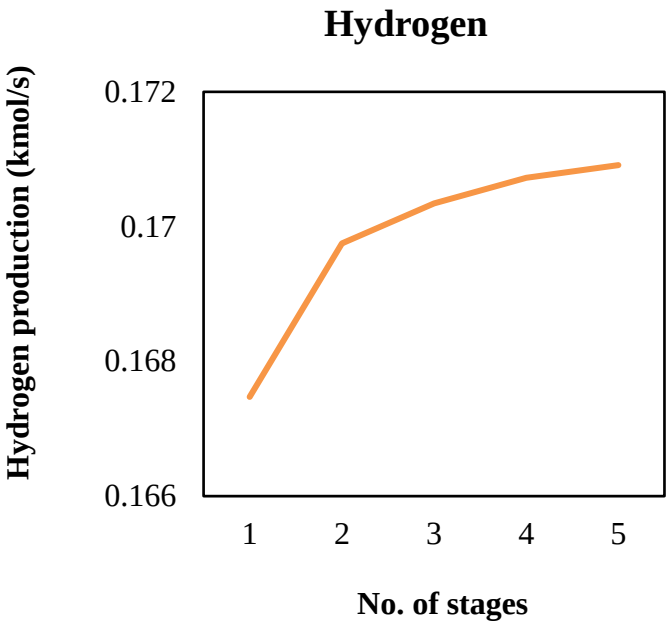

(c)

Figure 4.12 ***(cont.)*****:** Effect of number of stages on FBMR (b) aromatic production and (c) hydrogen production

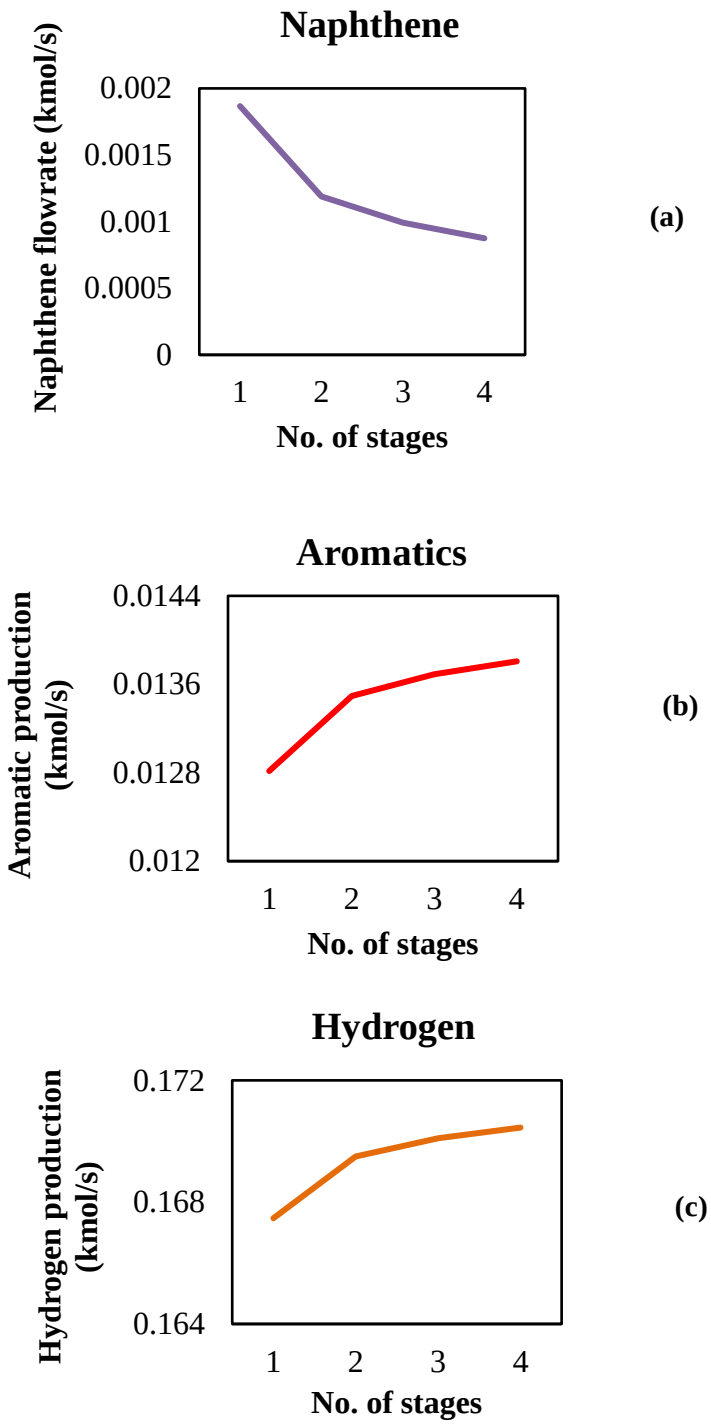

Figure 4.13: Effect of number of stages on FBR (a) Naphthene flowrate, (b) aromatic production and (c) hydrogen production

Chapter-5

Results and Discussion

A number of variables affect the catalyst performance. The results of this study evaluated the effect of varying different parameters on the reactor performance. The more important parameters are the temperature at which reaction is carried out, pressure of the shell side, properties of the naphtha feed and hydrogen to hydrocarbon molar ratio.

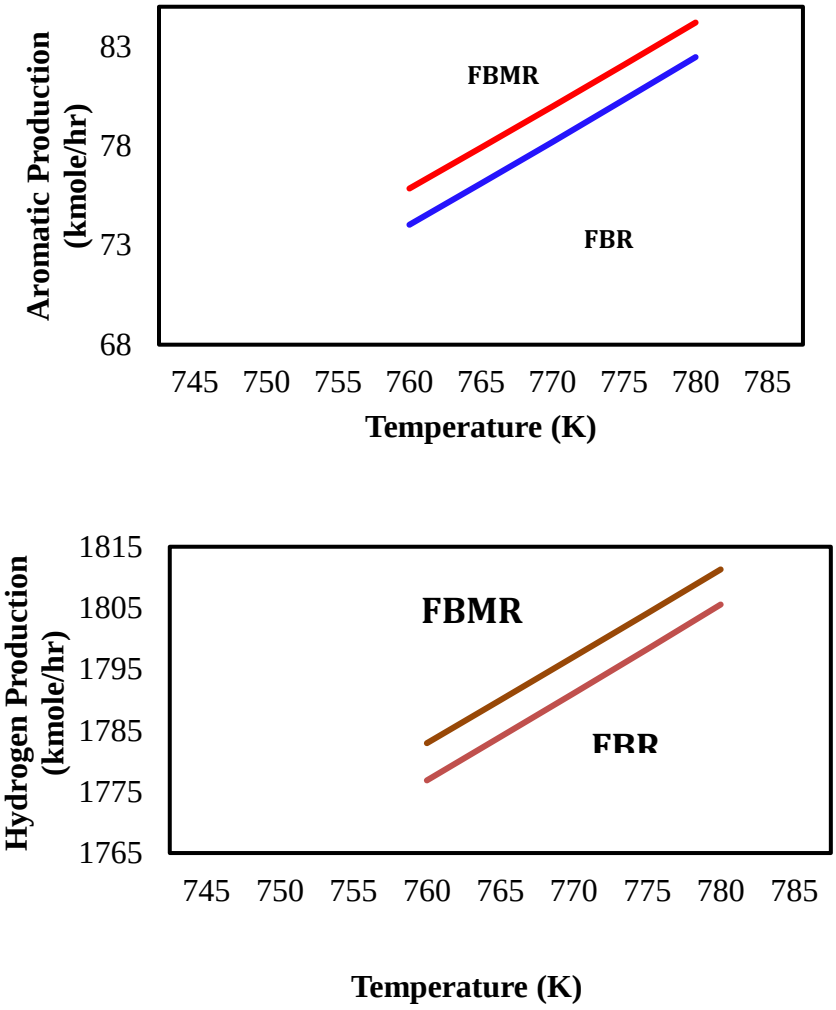

Figure 5.1: Effect of temperature on (a) aromatic production, (b) hydrogen production

5.1 Influence of Reactor Temperature

Endothermic reactions improve in yield as the temperature is raised. The dehydrogenation reaction is a highly endothermic and thus high temperature favors it. In Figure 5.1 (a) it is shown that a rise in temperature has a favorable impact on aromatic mole fraction. As the reaction proceeds inside the reactor due to its endothermic nature the temperature will drop and reaction rate will decrease. Further contact with catalyst will not produce any further increase in products due to the slowing of reaction with this decrease in temperature.

Figure 5.1 (b) Shows the effect of temperature on hydrogen production in both reactors. The rising trend shows that with the rise in temperature the hydrogen amount produced increases in both reactors but the total amount produced is more in case of the FBMR. This can be explained due to the selective removal of hydrogen, which is a product of reaction, and driving of the reaction to the product side

5.2 Influence of shell-side pressure

The second parameter to be evaluated is the shell side pressure. The difference between reaction side and permeate side pressure creates a driving force for hydrogen permeation. As the dehydrogenation reaction is hydrogen producer, with the reaction proceeding more hydrogen will be produced. In the case of FBR this hydrogen accumulates inside the reactor and increases its partial pressure and increase the affinity for products to move towards right side i.e. increasing the moles of reactants. The results are plotted in Figure 5.2 (a) and (b).

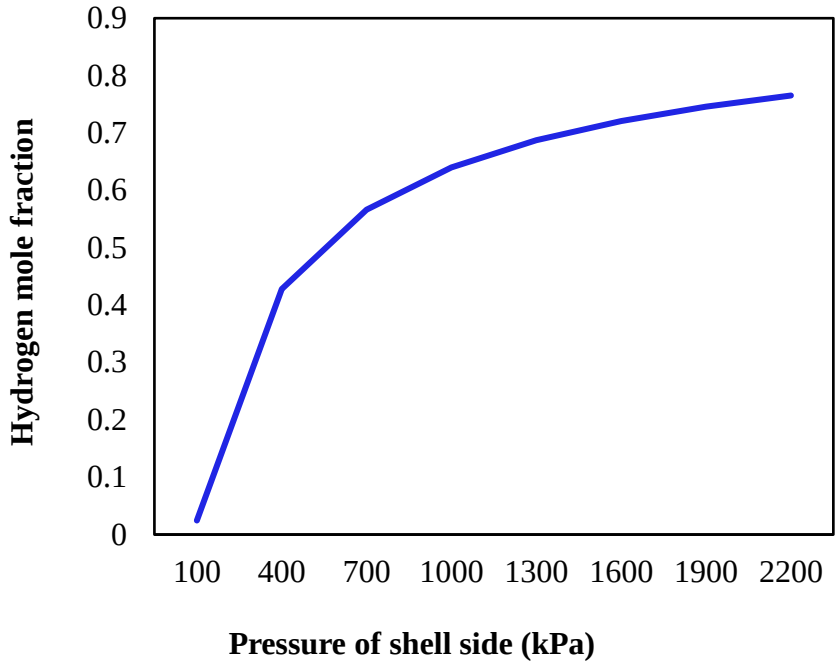

(a)

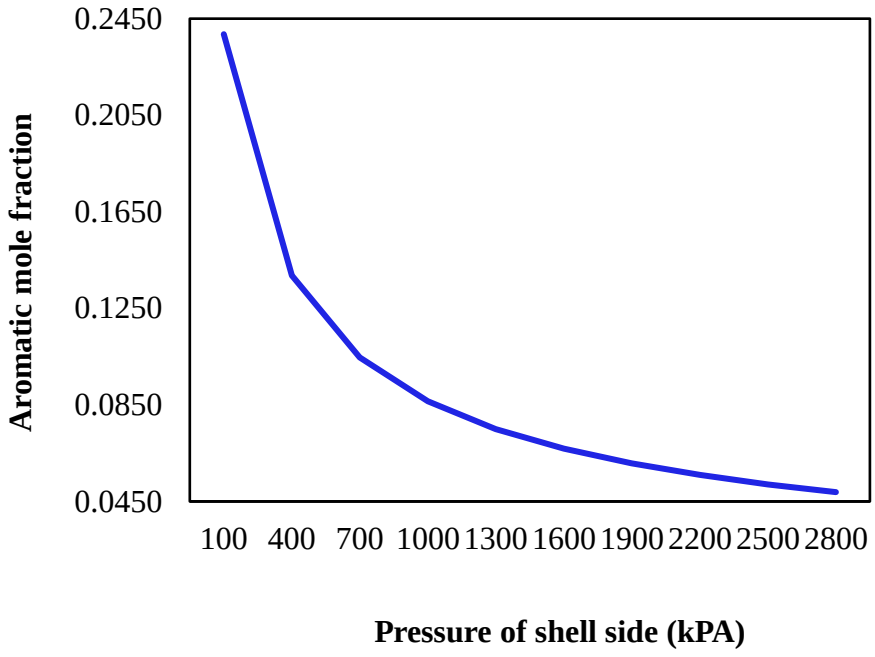

(b)

Figure 5.2: (a) Mole fraction of aromatic and (b) mole fraction of outlet hydrogen in reaction side as a function of shell side pressure.

But in the case of the membrane reactor the excess hydrogen is removed alongside the wall and thus keep its partial pressure constant or even decreasing it if the shell side pressure is further reduced. This is the main reason that the FBMR produces more aromatics as

compared to an FBR due to increased rate of forward reaction. Also a good quantity of ultrapure hydrogen is available for fuel cell application from the FBMR. While the pressure inside the reactor is controlled within narrow limits the pressure inside the shell can be varied and hydrogen and thus aromatic production can be controlled in an FBMR.

5.3 Influence of membrane thickness

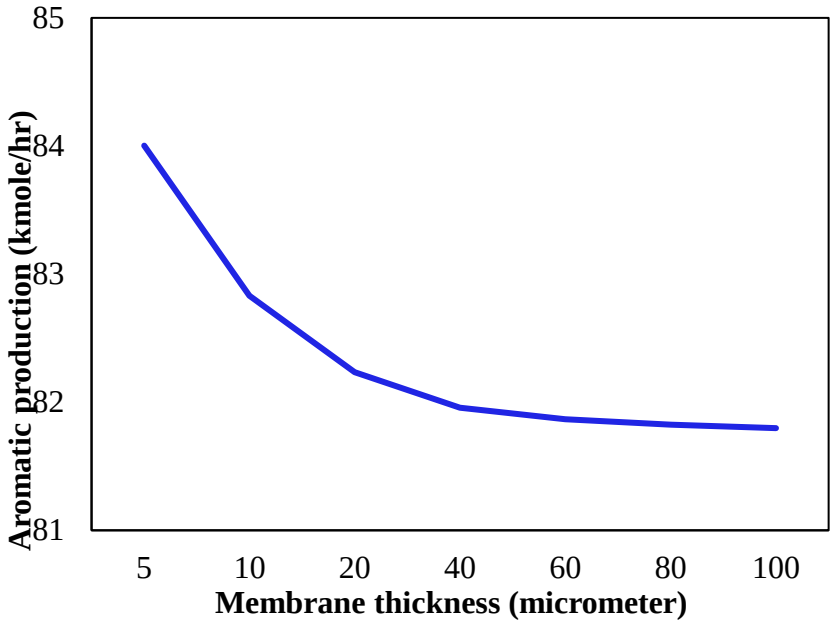

Figure 5.3: Effect of membrane thickness on production of aromatics

Third parameter to be evaluated is the membrane thickness. It was investigated the effect of membrane thickness molar aromatic production. Result is plotted in Figure 5.3. It can be clearly seen that when the membrane is very thin around 10 microns, aromatic production shows a sharp increase with further reduction in thickness. Furthermore, it is also observed that when the thickness is about 20 microns, further increase in thickness does not bring any significant reduction in aromatic molar production. Thin membrane requires a support material. Stainless steel and alumina are the more frequently used materials for this purpose. Alloying with silver is also a technique to provide mechanical strength.

5.4 Influence of H_2/Hc

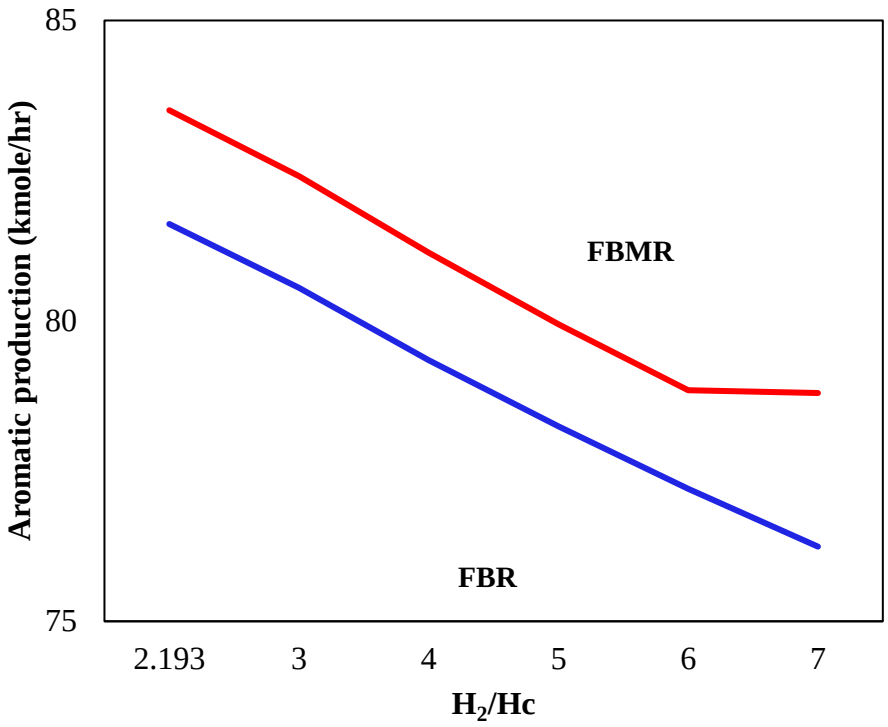

Figure 5.4: Effect of H_2/Hc molar ratio on aromatic production

The naphtha reforming reactions proceed under a hydrogen atmosphere to suppress the cracking reactions. The hydrogen to hydrocarbon molar ratio is an important parameter from an industrial stand point and its variation on aromatic production is included in this study. Higher H2/Hc ratios result in a milder reaction condition inside the reformer as hydrogen removes coke precursor from the catalyst surface. On the other hand, higher ratios mean lower aromatic molar production which can be seen in Figure 5.4. Here the advantage of membrane becomes clear. The effect of high H2/Hc ratio is more in the case of FBR as compared with an FBMR due to in situ hydrogen removal. The reason behind this is the accumulation of product hydrogen in the FBR. In the case of the FBMR a part of the hydrogen is continuously removed resulting in higher product concentration.

Table 5.1: Comparison between FBMR and FBR production rate

Pseudo components	Molecular weight	Input plant (mole fraction)	Output FBMR (kmol/hr)	Output FBR (kmol/hr)
Methane	16.043	0.008923	21.8072	22.3506
Ethane	30.070	0.009769	20.1581	20.3231
Propane	44.097	0.008542	16.4059	16.4059
N-Butane	58.124	0.004482	8.60898	8.6089
Isobutane	72.151	0.003087	5.92894	5.9289
N-pentane	58.124	0.001480	2.84258	2.8426
2-Methyl-Butane	72.150	0.003214	6.17255	6.1725
N-Hexane	86.178	0.009684	16.6844	16.5361
2-Methyl-Pentane	86.178	0.009811	16.9468	16.799
N-Heptane	100.20	0.012348	21.2363	21.0446
2-Methylhexane	100.21	0.013272	22.8735	22.6698
N-Octane	114.23	0.010107	13.4165	13.0649
2,2,4-Trimethylpentane	114.23	0.014294	19.3122	18.8262
N-Nonane	128.26	0.006597	11.2296	11.1195
2,2,5-Trimethylhexane	128.26	0.010318	17.6938	17.5306
Cyclohexane	84.162	0.003256	5.94071	5.9161
Methylcyclohexane	98.189	0.003552	6.44809	6.4188
Ethylcyclohexane	112.22	0.004863	7.75668	7.6494
N-Propylcyclohexane	126.24	0.000761	1.38288	1.37671
Cyclopentane	70.135	0.000042	0.08121	0.0812
Methylcyclopentane	84.162	0.001268	2.43626	2.4362
Ethylcyclopentane	98.189	0.002749	5.27823	5.2781
N-propylyclopentane	112.22	0.003552	6.82105	6.8209
N-Butylclopentane	126.24	0.000508	0.97443	0.9744
Benzene	78.114	0.003637	14.6462	15.3824
Toluene	92.140	0.004609	13.0969	13.3763
M-Xylene	106.17	0.000634	5.10964	5.3425
O-Xylene	106.17	0.000676	6.19122	6.5296
P-Xylene	106.17	0.001522	6.04034	6.1834
Ethylbenzene	106.17	0.000888	4.85127	4.9975
N-Propylbenzene	120.20	0.001099	4.12782	4.2211
Hydrogen	2.0160	0.840438	1721.48	1728.487

Tables 5.1 is the output from the first phase of FBMR and FBR. First column shows the components chosen from the Aspen PLUS database to represent the hydrocarbon. Second column is the mole fraction of that component in the feed. Next two columns show the output from the FBMR and FBR phase.

Table 5.2 shows the output from the second phase the FBMR and FBR as reported by the Aspen PLUS simulator. The reactants are partially converted into products and the output from second phase is combined. In the FBMR hydrogen is removed and then products become input to the next phase.

Table 5.2: Comparison between FBMR and FBR production rate

Pseudo components	Molecular weight	Input plant (mole fraction)	Output FBMR (kmol/hr)	Output FBR (kmol/hr)
Methane	16.043	0.008923	24.1132	24.7254
Ethane	30.070	0.009769	20.8704	21.0558
Propane	44.097	0.008542	16.4059	16.4059
N-Butane	58.124	0.004482	8.6089	8.6089
Isobutane	72.151	0.003087	5.9289	5.9289
N-pentane	58.124	0.001480	2.8425	2.8425
2-Methyl-Butane	72.150	0.003214	6.1725	6.1725
N-Hexane	86.178	0.009684	15.9311	15.78271
2-Methyl-Pentane	86.178	0.009811	16.2000	16.0524
N-Heptane	100.20	0.012348	20.2618	20.0701
2-Methylhexane	100.21	0.013272	21.8393	21.6355
N-Octane	114.23	0.010107	11.3716	11.0597
2,2,4-Trimethylpentane	114.23	0.014294	16.5052	16.0706
N-Nonane	128.26	0.006597	10.6665	10.5569
2,2,5-Trimethylhexane	128.26	0.010318	16.8606	16.6972
Cyclohexane	84.162	0.003256	5.8183	5.7934
Methylcyclohexane	98.189	0.003552	6.3020	6.2725
Ethylcyclohexane	112.22	0.004863	7.1766	7.0740
N-Propylcyclohexane	126.24	0.000761	1.3520	1.3457
Cyclopentane	70.135	0.000042	0.0812	0.0812
Methylcyclopentane	84.162	0.001268	2.4361	2.4361
Ethylcyclopentane	98.189	0.002749	5.2779	5.2779
N-propylyclopentane	112.22	0.003552	6.8206	6.8206
N-Butylclopentane	126.24	0.000508	0.9743	0.9743
Benzene	78.114	0.003637	18.0161	18.807
Toluene	92.140	0.004609	14.6747	14.933
M-Xylene	106.17	0.000634	6.45162	6.660
O-Xylene	106.17	0.000676	8.0153	8.3395
P-Xylene	106.17	0.001522	6.9873	7.0959
Ethylbenzene	106.17	0.000888	5.8132	5.9251
N-Propylbenzene	120.20	0.001099	4.7420	4.8130
Hydrogen	2.0160	0.840438	1760.13	1766.672

The products from the second phase are input to the next phase. Table 5.3 shows the output from third phase. The naphtha feed has further reacted to convert naphthenes present in the feed to aromatics which are the desirable products.

Table 5.3: Comparison between FBMR and FBR production rate

Pseudo components	Molecular weight	Input plant (mole fraction)	Output FBMR (kmol/hr)	Output FBR (kmol/hr)
Methane	16.043	0.008923	25.6052	26.2021
Ethane	30.070	0.009769	21.3339	21.5136
Propane	44.097	0.008542	16.4059	16.40593
N-Butane	58.124	0.004482	8.6089	8.6089
Isobutane	72.151	0.003087	5.9289	5.9289
N-pentane	58.124	0.001480	2.8425	2.8425
2-Methyl-Butane	72.150	0.003214	6.1725	6.1725
N-Hexane	86.178	0.009684	15.4915	15.3555
2-Methyl-Pentane	86.178	0.009811	15.7638	15.6285
N-Heptane	100.20	0.012348	19.6932	19.5179
2-Methylhexane	100.21	0.013272	21.2356	21.0492
N-Octane	114.23	0.010107	10.2577	9.9953
2,2,4-Trimethylpentane	114.23	0.014294	14.9683	14.6004
N-Nonane	128.26	0.006597	10.3387	10.2389
2,2,5-Trimethylhexane	128.26	0.010318	16.3747	16.2256
Cyclohexane	84.162	0.003256	5.7473	5.7241
Methylcyclohexane	98.189	0.003552	6.2175	6.1900
Ethylcyclohexane	112.22	0.004863	6.8504	6.7586
N-Propylcyclohexane	126.24	0.000761	1.33416	1.3283
Cyclopentane	70.135	0.000042	0.08121	0.0812
Methylcyclopentane	84.162	0.001268	2.43614	2.4361
Ethylcyclopentane	98.189	0.002749	5.27780	5.27775
N-propylyclopentane	112.22	0.003552	6.82047	6.8204
N-Butylclopentane	126.24	0.000508	0.97434	0.97434
Benzene	78.114	0.003637	20.09485	20.8498
Toluene	92.140	0.004609	15.56115	15.7843
M-Xylene	106.17	0.000634	7.1865	7.3637
O-Xylene	106.17	0.000676	9.0597	9.3463
P-Xylene	106.17	0.001522	7.4625	7.5440
Ethylbenzene	106.17	0.000888	6.3000	6.3838
N-Propylbenzene	120.20	0.001099	5.0477	5.1014
Hydrogen	2.0160	0.840438	1781.73	1787.446845

The reactions occur in both PFR and CSTR which represent the bubble and emulsion phases respectively. Most of the catalyst is in the CSTR. The PFR has a very less

quantity of catalyst and so the reactions rate is very low. As the bubble phase is dispersed within the emulsion phase, products from the PFR have a chance to move into the CSTR. This mass transfer allows the unreacted material to react in the CSTR thus improving the reactor effectiveness. Table 5.4 show the species concentration in the fourth phase.

Table 5.4: Comparison between FBMR and FBR production rate

Pseudo components	Molecular weight	Input plant (mole fraction)	Output FBMR (kmol/hr)	Output FBR (kmol/hr)
Methane	16.043	0.008923	26.7049	27.2619
Ethane	30.070	0.009769	21.6758	21.8428
Propane	44.097	0.008542	16.4059	16.4059
N-Butane	58.124	0.004482	8.6089	8.6089
Isobutane	72.151	0.003087	5.9289	5.9289
N-pentane	58.124	0.001480	2.8425	2.8425
2-Methyl-Butane	72.150	0.003214	6.1725	6.1725
N-Hexane	86.178	0.009684	15.1877	15.0654
2-Methyl-Pentane	86.178	0.009811	15.4623	15.3405
N-Heptane	100.20	0.012348	19.3004	19.1429
2-Methylhexane	100.21	0.013272	20.8185	20.6509
N-Octane	114.23	0.010107	9.5204	9.3004
2,2,4-Trimethylpentane	114.23	0.014294	13.9478	13.6376
N-Nonane	128.26	0.006597	10.1126	10.0233
2,2,5-Trimethylhexane	128.26	0.010318	16.0392	15.9054
Cyclohexane	84.162	0.003256	5.6987	5.6773
Methylcyclohexane	98.189	0.003552	6.1595	6.1343
Ethylcyclohexane	112.22	0.004863	6.6308	6.5484
N-Propylcyclohexane	126.24	0.000761	1.3219	1.3165
Cyclopentane	70.135	0.000042	0.0812	0.0812
Methylcyclopentane	84.162	0.001268	2.436	2.4361
Ethylcyclopentane	98.189	0.002749	5.27771	5.2776
N-propylyclopentane	112.22	0.003552	6.8203	6.8202
N-Butylclopentane	126.24	0.000508	0.9743	0.9743
Benzene	78.114	0.003637	21.5839	22.281
Toluene	92.140	0.004609	16.1555	16.347
M-Xylene	106.17	0.000634	7.6746	7.8244
O-Xylene	106.17	0.000676	9.7748	10.0237
P-Xylene	106.17	0.001522	7.7581	7.8204
Ethylbenzene	106.17	0.000888	6.6043	6.6684
N-Propylbenzene	120.20	0.001099	5.2351	5.2776
Hydrogen	2.0160	0.840438	1796.2470	1801.2112

As the reactions inside the bed proceeds more naphthenes in the feed are converted to aromatics thus further increasing the reformate quality. Table 5.5 shows the composition of the fifth phase. Reaction is now almost complete and rate of reaction has decreased.

Table 5.5: Comparison between FBMR and FBR production rate

Pseudo components	Molecular weight	Input plant (mole fraction)	Output FBMR (kmol/hr)	Output FBR (kmol/hr)
Methane	16.043	0.008923	27.5788	27.2619
Ethane	30.070	0.009769	21.9475	21.8423
Propane	44.097	0.008542	16.4059	16.4059
N-Butane	58.124	0.004482	8.608	8.6089
Isobutane	72.151	0.003087	5.928	5.9289
N-pentane	58.124	0.001480	2.842	2.8425
2-Methyl-Butane	72.150	0.003214	6.172	6.1725
N-Hexane	86.178	0.009684	14.9578	15.0654
2-Methyl-Pentane	86.178	0.009811	15.2341	15.3405
N-Heptane	100.20	0.012348	19.0032	19.1429
2-Methylhexane	100.21	0.013272	20.5028	20.6509
N-Octane	114.23	0.010107	8.9799	9.30040
2,2,4-Trimethylpentane	114.23	0.014294	13.1981	13.6376
N-Nonane	128.26	0.006597	9.9415	10.0233
2,2,5-Trimethylhexane	128.26	0.010318	15.7852	15.9054
Cyclohexane	84.162	0.003256	5.6621	5.6773
Methylcyclohexane	98.189	0.003552	6.1159	6.1343
Ethylcyclohexane	112.22	0.004863	6.4677	6.5489
N-Propylcyclohexane	126.24	0.000761	1.3126	1.3165
Cyclopentane	70.135	0.000042	0.0812	0.0812
Methylcyclopentane	84.162	0.001268	2.4361	2.4361
Ethylcyclopentane	98.189	0.002749	5.2776	5.2776
N-propylyclopentane	112.22	0.003552	6.8202	6.8202
N-Butylclopentane	126.24	0.000508	0.9743	0.9743
Benzene	78.114	0.003637	22.7430	22.2810
Toluene	92.140	0.004609	16.5940	16.3472
M-Xylene	106.17	0.000634	8.0331	7.8244
O-Xylene	106.17	0.000676	10.3133	10.0237
P-Xylene	106.17	0.001522	7.9623	7.8204
Ethylbenzene	106.17	0.000888	6.8165	6.6684
N-Propylbenzene	120.20	0.001099	5.36288	5.2776
Hydrogen	2.0160	0.840438	1807.0000	1801.2112

In this phase the quantity of naphthenes has reduced significantly due to their conversion into aromatics that have increased significantly. Dehydrogenation reactions are the major reforming reactions and produce a lot of hydrogen as a useful byproduct. More quantity of hydrogen and aromatics is produced from the FBMR when compared with the FBR as evident from Table 5.5.

Table 5.6: Parameters for FBMR and FBR

	FBMR			FBR	
	In	Out	Out H_2	In	Out
Temperature, K	777	656	680	777	667
Pressure, MPa	3.703	3.703	0.9	3.703	3.703
Flowrate, Kg/hr	30410	28561	1849	30410	30410
Molar Enthalpy, KJ/mol	4.83	-3.09	11.18	4.83	3.25
Molar Entropy, J/mol-K	-54033.8	-84841.9	5936.7	-54033.8	-49834.3

Table 5.6 details the important parameters of the FBMR and FBR. Temperature, pressure and feed flowrate are the more important variables that affect the reactor performance. The pressure of the reactor is fixed after and cannot be varied except within a slight margin. This leaves the temperature and feed flowrate the primary manipulated variables. Higher temperature results in higher aromatic production with the upper limit set by the metallurgy of the system. There is no separate stream of hydrogen from the FBR and it is combined with the reformate.

Table 5.7: Comparison of FBMR and FBR in terms of hydrogen and aromatics production

		FBR	FBMR	Increase from using membrane	
	Feed kg/hr	Out kg/hr	Out kg/hr	Daily increase kg/day	Yearly increase kg/Yr.
Hydrogen	3254	3631	3643	280	102329
Aromatics	2374	7437	7467	720	262800

In Table 5.7 the output from both the FBMR and FBR is compared. The first column shows the quantity of hydrogen and aromatics in the feed. The second and third column shows the production rate of respective component. The calculated daily and yearly increase in aromatic and hydrogen is tabulated in the last two columns for comparison.

In this study a semi-regenerative type of reformer was modelled and simulated. A Pt/Re type catalyst on chlorided alumina support is used in the industrial semi-regenerative reformers. Other types of reformers such as the continuous catalyst recirculation type reformer uses a platinum doped with tin catalyst due to its harsher environment. A catalyst promotes both forward and reverse reaction but it cannot change the position of equilibrium. The thermodynamics of the reaction solely governs the equilibrium concentration of products. To promote the reaction further heating of the reaction mixture is required thus the reaction is carried out in three separate adiabatic reactor vessels with varying catalyst amount and inter-stage heaters are provided to reheat the product stream to the reaction temperature [2].

Conclusions and Recommendations

A fluidized-bed naphtha reformer with in situ membrane separation model was developed in the Aspen PLUS environment. The hydrodynamic parameters and membrane permeation phenomena were implemented using Excel interfacing. The results of the FBMR were compared with a simple fluidized bed reactor (FBR). It was observed that hydrogen removal from the permeate side drove the reaction forward and resulted in an increase of the aromatic yield. In addition, hydrogen production also increased due to its simultaneous separation during the reaction.

The endothermic nature of the dehydrogenation reaction causes a sharp drop in temperature inside the reactor while operating in the adiabatic mode. One of the benefits of using the fluidized bed reactor is its superior heat transfer characteristics. Use of external heating coils can be implemented for converting the reactor to the iso thermal mode. This mode cannot be used in packed bed reactors due to difficulty and complex nature of internal heating arrangements.

This work shows that the FBMR outperformed the FBR in terms of output of both hydrogen and aromatics. Before this process is up scaled for industrial production a comparative cost analysis of the membrane material against the extra profit from increased production is required. Another important factor is the study on how long the membrane material will survive the harsh and erosive environment present inside the fluidized bed.

References

[1]. Antos, G. J., & Aitani, A. M. (2004). Catalytic naphtha reforming, revised and expanded. CRC Press.

[2]. Ancheyta, J. (2011). Modeling and simulation of catalytic reactors for petroleum refining. John Wiley & Sons.

[3]. Rahimpour, M. R., Jafari, M., & Iranshahi, D. (2013). Progress in catalytic naphtha reforming process: A review. Applied energy, 109, 79-93.

[4]. Patil, C. S., van Sint Annaland, M., & Kuipers, J. A. (2005). Design of a novel autothermal membrane-assisted fluidized-bed reactor for the production of ultrapure hydrogen from methane. Industrial & engineering chemistry research, 44(25), 9502-9512.

[5]. Barbieri, G., Marigliano, G., Perri, G., & Drioli, E. (2001). Conversion− temperature diagram for a palladium membrane reactor. Analysis of an endothermic reaction: Methane steam reforming. Industrial & engineering chemistry research, 40(9), 2017-2026.

[6]. Wieland, S., Melin, T., & Lamm, A. (2002). Membrane reactors for hydrogen production. Chemical Engineering Science, 57(9), 1571-1576.

[7]. Howard, B. H., Killmeyer, R. P., Rothenberger, K. S., Cugini, A. V., Morreale, B. D., Enick, R. M., & Bustamante, F. (2004). Hydrogen permeance of palladium–copper alloy membranes over a wide range of temperatures and pressures. Journal of Membrane Science, 241(2), 207- 218.

[8]. Barbieri, G., & Di Maio, F. P. (1997). Simulation of the methane steam re-forming process in a catalytic Pd-membrane reactor. Industrial & engineering chemistry research, 36(6), 2121-2127.

[9]. Shu, J., Grandjean, B. P., & Kaliaguine, S. (1994). Methane steam reforming in asymmetric Pd-and Pd-Ag/porous SS membrane reactors. Applied Catalysis A: General, 119(2), 305-325.

[10]. Keuler, J. N., & Lorenzen, L. (2002). Comparing and Modeling the

[11]. Dehydrogenation of Ethanol in a Plug-Flow Reactor and a Pd− Ag Membrane

Reactor. Industrial & engineering chemistry research, 41(8), 1960-1966.

[12]. Gobina, E. N., Oklany, J. S., & Hughes, R. (1995). Elimination of ammonia from coal gasification streams by using a catalytic membrane reactor. Industrial & engineering chemistry research, 34(11), 3777-3783.

[13]. Rahimpour, M. R., & Ghader, S. (2003). Theoretical investigation of a membrane reactor for methanol synthesis. Chemical Engineering & Technology: Industrial Chemistry-Plant Equipment-Process Engineering Biotechnology, 26(8), 902-907.

[14]. Tosti, S., Basile, A., Bettinali, L., Borgognoni, F., Gallucci, F., & Rizzello, C. (2008). Design and process study of Pd membrane reactors. International Journal of Hydrogen Energy, 33(19), 5098-5105.

[15]. Roy, S., Cox, B. G., Adris, A. M., & Pruden, B. B. (1998). Economics and simulation of fluidized bed membrane reforming. International journal of hydrogen energy, 23(9), 745-752.

[16]. Mostafazadeh, A. K., & Rahimpour, M. R. (2009). A membrane catalytic bed concept for naphtha reforming in the presence of catalyst deactivation. Chemical Engineering and Processing: Process Intensification, 48(2), 683-694.

[17]. Rahimpour, M. R. (2009). Enhancement of hydrogen production in a novel fluidized-bed membrane reactor for naphtha reforming. International Journal of Hydrogen Energy, 34(5), 2235-2251.

[18]. Rahimpour, M. R., Vakili, R., Pourazadi, E., Iranshahi, D., & Paymooni, K. (2011). A novel integrated, thermally coupled fluidized bed configuration for catalytic naphtha reforming to enhance aromatic and hydrogen productions in refineries. international journal of hydrogen energy, 36(4), 2979-2991.

[19]. Grace, J. R., Li, X., & Lim, C. J. (2001). Equilibrium modelling of catalytic steam reforming of methane in membrane reactors with oxygen addition. Catalysis today, 64(3-4), 141-149.

[20]. Sarvar-Amini, A., Sotudeh-Gharebagh, R., Bashiri, H., Mostoufi, N., & Haghtalab, A. (2007). Sequential simulation of a fluidized bed membrane reactor for the steam methane reforming using Aspen PLUS. Energy &

Fuels, 21(6), 3593-3598.

[21]. Ye, G., Xie, D., Qiao, W., Grace, J. R., & Lim, C. J. (2009). Modeling of fluidized bed membrane reactors for hydrogen production from steam methane reforming with Aspen Plus. International journal of hydrogen energy, 34(11), 4755-4762.

[22]. Benitez, V. M., & Pieck, C. L. (2010). Influence of indium content on the properties of Pt–Re/Al2O3 naphtha reforming catalysts. Catalysis letters, 136(1-2), 45-51.

[23]. Mazzieri, V. A., Pieck, C. L., Vera, C. R., Yori, J. C., & Grau, J. M. (2009). Effect of Ge content on the metal and acid properties of Pt-Re-Ge/Al2O3-Cl catalysts for naphtha reforming. Applied Catalysis A: General, 353(1), 93-100.

[24]. Benitez, V., Boutzeloit, M., Mazzieri, V. A., Especel, C., Epron, F., Vera, C. R., ... & Pieck, C. L. (2007). Preparation of trimetallic Pt–Re–Ge/Al2O3 and Pt–Ir–Ge/Al2O3 naphtha reforming catalysts by surface redox reaction. Applied Catalysis A: General, 319, 210-217.

[25]. Smith R. Kinetic analysis of naphtha reforming with platinum catalyst. Chem Eng Prog 1959; 55:76–80.

[26]. Marin, G. B., Froment, G. F., Lerou, J. J., & De Backer, W. (1983). Simulation of a catalytic naphtha reforming unit.

[27]. Froment G. The kinetic of complex catalytic reactions. Chem Eng Sci 1987; 42:1073.

[28]. Ramage MP, Graziani KR, Krubeck FJ. Development of Mobil's kinetic reforming model. Chem Eng Sci 1980; 35:41–8.

[29]. Ancheyta-Juarez J, Villafuerte-Macias E. Kinetic modeling of naphtha catalytic reforming reactions. Energy Fuels 2000; 14:1032–7.

[30]. Hu Y, Xu W, Su H, Chu J. A dynamic model for naphtha catalytic reformers. In: International conference on control applications, Taipei, Taiwan; 2004

[31]. Weifeng H, Hongye S, Yongyou U, Jian C. Modeling, simulation and optimization of a whole industrial catalytic naphtha reforming process on Aspen Plus platform. Chin J Chem Eng 2006; 14:584–91.

[32]. Vathi GP, Chaughuri KK. Modelling and simulation of commercial catalytic

naphtha reformers. Can J Chem Eng 1997; 75:930–7.

[33]. Modeling and Simulation of a Novel Membrane Reactor in Continuous Catalytic Regenerative (CCR) Naphtha Reformer Accompanied with Detailed Description of Kinetic Davood Iranshahi, Shahram Amiri, Mohsen Karimi, Razieh Rafiei, Mitra Jafari, and Mohammad Reza Rahimpour

[34]. Pasha, Mustafa & Ahmad, Iftikhar & Mustafa, Jawad & Kano, Manabu. (2018). Modeling of a Nickel-based Fluidized Bed Membrane Reactor for Steam Methane Reforming Process. Journal- Chemical Society of Pakistan.

[35]. Porrazzo, R., White, G., & Ocone, R. (2014). Aspen PLUS simulations of fluidised beds for chemical looping combustion. Fuel, 136, 46-56.

[36]. Fazeli, A., Fatemi, S., Mahdavian, M., & Ghaee, A. (2009). Mathematical modeling of an industrial naphtha reformer with three adiabatic reactors in series. Iranian Journal of Chemistry and Chemical Engineering (IJCCE), 28(3), 97-102.

[37]. Krane, H. G., Groh, A. B., Schulman, B. L., & Sinfelt, J. H. (1959, January 1). 4. Reactions in Catalytic Reforming of Naphthas. World Petroleum Congress.

[38]. Kmak, W. S., & Stuckey, A. N. (1973). Powerforming process studies with a kinetic simulation model. AlChE National Meetmg, New Orleans, March, Paper No. 56a.

[39]. Lee, J. W., Ko, Y. C., Jung, Y. K., Lee, K. S., & Yoon, E. S. (1997). A modeling and simulation study on a naphtha reforming unit with a catalyst circulation and regeneration system. Computers & chemical engineering, 21, S1105-S1110.

[40]. Lid, T., & Skogestad, S. (2008). Data reconciliation and optimal operation of a catalytic naphtha reformer. Journal of Process Control, 18(3-4), 320-331.